JOURNAL OF GEOPHYSICAL RESEARCH, VOL. 106, NO. B2, PAGES 2245–2263, FEBRUARY 10, 2001

Refined kinematics of the Eastern California shear zone from GPS observations, 1993-1998

M. Meghan Miller and Daniel J. Johnson

Department of Geological Sciences, Central Washington University, Ellensburg, Washington

Timothy H. Dixon

Division of Marine Geology and Geophysics, Rosenstiel School of Marine and Atmospheric Sciences, University of Miami, Miami, Florida

Roy K. Dokka

Department of Geology and Geophysics, Louisiana State University, Baton Rouge, Louisiana

Abstract. Global Positioning System (GPS) results from networks spanning the Eastern California shear zone and adjacent Sierra Nevada block, occupied annually between 1993 and 1998, constrain plate margin kinematics. We use an elastic block model to relate GPS station velocities to long-term fault slip rate estimates. The model accounts for elastic strain accumulation on the San Andreas fault, as well as faults of the Eastern California shear zone. South of the Garlock fault, 14 mm/yr of dextral shear is distributed across the Eastern California shear zone. Some of this slip penetrates eastward into the Basin and Range, and a collective budget of 13 mm/yr is observed to the north at the latitude of Owens Lake. Model slip rates for two important faults, the Garlock and Owens Valley faults, significantly misfit geologic estimates. By referencing station velocities to stable North America we observe northward-increasing deformation east of our regional GPS network. At the latitude of Mojave Desert, however, some of this deformation is ascribed to elastic strain accumulation due to a locked San Andreas fault and thus does not represent additional fault-related, permanent deformation.

1. Introduction

The San Andreas fault system forms the transform boundary that separates the North America and Pacific plates at the latitude of California, but deformation occurs in a zone much broader than the fault itself [*Atwater*, 1970] (Figure 1). Estimates of relative plate motion over geologic and geodetic timescales [*Stock and Molnar*, 1989; *DeMets et al.*, 1990, 1994; *DeMets*, 1995; *Larson et al.*, 1997; *DeMets and Dixon*, 1999] and detailed accounting of slip from geologic and geodetic techniques [*Bird and Rosenstock*, 1984; *Weldon and Humphreys*, 1986; *Dokka and Travis*, 1990a, 1990b; *Humphreys and Weldon*, 1994; *Argus and Gordon*, 1996; *Hearn and Humphreys*, 1998] now describe the kinematics of this deforming continental margin. Deformation of the western edge of North America results from its interaction with the relatively rigid Pacific plate and the penetration of plate boundary shear into weaker and gravitationally unstable continental crust [*Atwater and Stock*, 1998].

The difference between relative plate motion in southern California (~50 mm/yr [*DeMets and Dixon*, 1999]) and slip rate determinations along the San Andreas fault (~35 mm/yr [*Sieh and Jahns*, 1984]), which was known as the San Andreas discrepancy [*DeMets et al.*, 1987], is now considered negligible with inclusion of deformation that occurs across the entire plate margin deformation zone [*Weldon and Humphreys*, 1986; *Feigl et al.*, 1993; *Humphreys and Weldon*, 1994; *Sauber et al.*, 1994] and with continued refinements in the estimated angular velocity for this plate pair.

The Eastern California shear zone plays a major role in balancing the discrepancy between predicted plate motion and San Andreas fault activity. Its importance was first suggested on the basis of patterns of historical seismicity in eastern California and Nevada [*Wallace*, 1984] (Figure 2). Geodesy [*Sauber et al.*, 1989; *Savage et al.*, 1990; *Sauber et al.*, 1994; *Dixon et al.*, 1995; *Gan et al.*, 2000] and geologic relations [*Dokka and Travis*, 1990a, 1990b] confirm its importance. The moniker Eastern California shear zone was first used for faults within the Mojave Desert [*Dokka and Travis*, 1990a, 1990b] but is now more broadly employed to include the penetration of through-going deformation north of the Garlock fault into the southern Walker Lane region (Figure 1).

Many large earthquakes have ruptured faults within this zone since 1872 (Figure 2), and several of these earthquakes have exceeded magnitude 6.8 (e.g., the 1872 Owens Valley, 1915 Pleasant Valley, 1932 Cedar Mountain, 1954 Dixie Valley–Fairview Peak, 1992 Landers, and 1999 Hector Mine earthquakes [*Wallace*, 1984; *Kanamori et al.*, 1992; *Scientists from the U.S. Geological Survey*, 2000]). Yet most of these faults show little evidence for recent or prehistoric activity, and the estimated recurrence interval of earthquakes of this size along the individual faults that have ruptured are as great as one thousand to 10,000 years [*Wallace*, 1984; *Rockwell et al.*, 1993; *Beanland and Clark*, 1994; *Petersen and Wesnousky*,

Paper number 2000JB900328.
0148-0227/01/2000JB900328$09.00

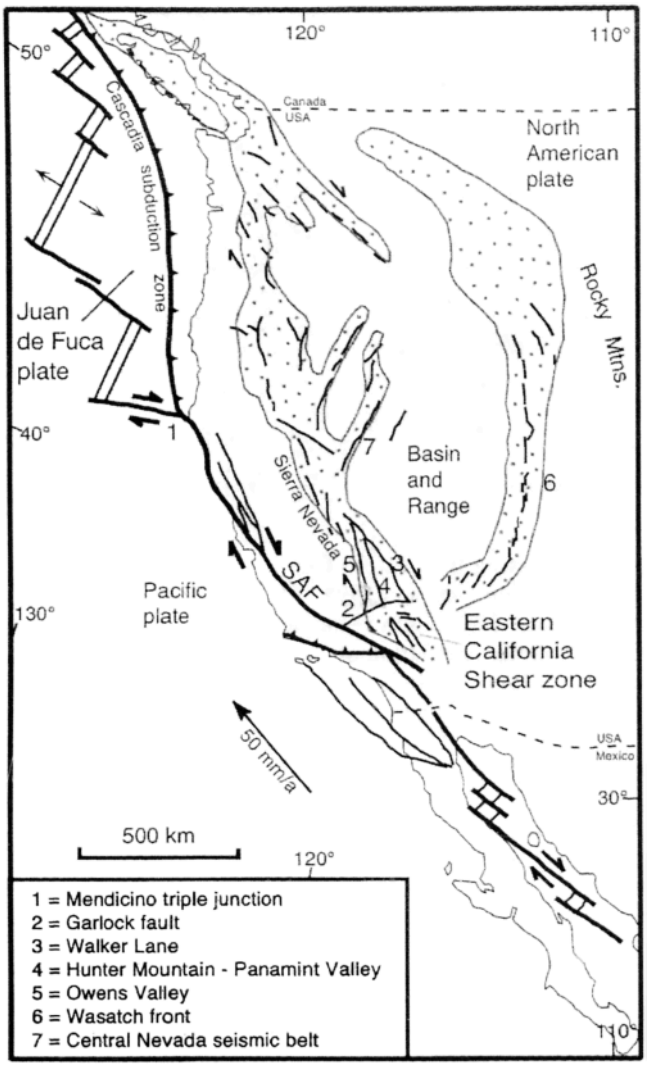

Figure 1. Tectonic setting of the Eastern California shear zone. Coastal California south of the Mendocino triple junction is exposed to transform motion between the Pacific and North America plates. As much as 28-29% of the relative plate motion penetrates into the plate margin east of the San Andreas fault. This motion is accommodated by dextral and normal faults of the Eastern California shear zone, which lie within the Mojave Desert and penetrates to the north, east of the Sierra Nevada. Smaller amounts of motion penetrate even farther to the east, along the Wasatch front. This deformation ultimately feeds into the back arc region of the Cascadia subduction zone, which lies north of the Mendocino triple junction. In the early 1990s we initiated GPS studies to quantify the budget and partitioning of the Eastern California shear zone kinematics. Figure modified from Pezzopane and Weldon [1993].

1994; *Rubin and Sieh*, 1997]. Because large earthquakes have historically filled gaps in this record along the Eastern California shear zone and central Nevada seismic belt [*Wallace*, 1984], future seismicity may be likely in remaining gaps. Specific vulnerable gaps occur along the White Mountains range front and the stretch of Landers earthquake aftershocks between Barstow and the southern Owens Valley (Figure 2).

This study presents new regional GPS constraints on deformation within the Eastern California shear zone and reveals its role in plate margin deformation. The GPS velocities are integrated into a geologically constrained model for plate margin related deformation. The goal of our modeling is to relate the instantaneous GPS velocity field to long-term or geologic deformation.

2. Methods

During 1991, we installed a high-precision GPS geodetic network that was augmented in subsequent years (Table 1), in order to measure secular strain associated with a complex continental transform margin, where slip is partitioned from the San Andreas fault northeastward through the Mojave Desert via the Eastern California shear zone to the Walker Lane [*Miller et al.*, 1992]. This network spans latitudes 33.5°-38°N, and characterizes slip distribution across the zone. This paper reports results from 1993 to 1998, in order to minimize coseismic and possible postseismic contamination of the velocity field by the 1992 $Mw = 7.3$ Landers earthquake, although these effects cannot be eliminated completely. The stations were observed

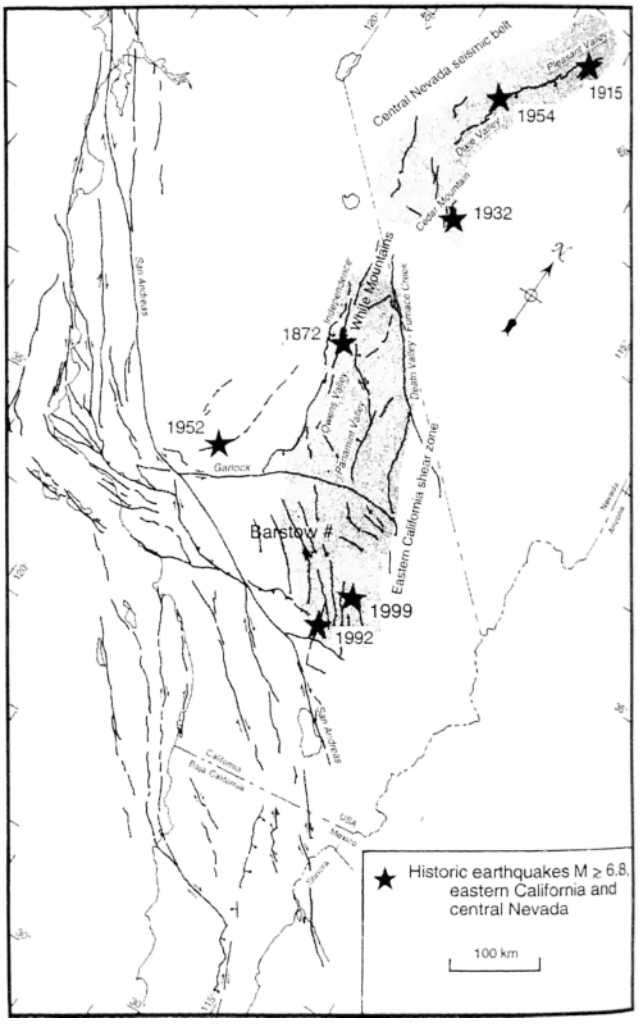

Figure 2. Large historic earthquakes within the western margin of the North America plate. These events define a zone of heightened seismicity during the last 125 years that defines the inland penetration of plate margin deformation. Modified from Wallace [1984].

Table 1. GPS Campaign Stations.

Staion ID	Station Name	Longitude, °E	Latitude, °N	Stamping	Monument Type	Agency Installed/Observed	Number of Days Each Year,[a]
ABER	Aberdeen	241.71170	36.97906	3200S	steel pin in rock	JPL/CWU	0,5,5,5,5,5
BAMA	Alabama Hills	241.88052	36.60256	3190S	steel pin in bedrock	JPL/CWU	5,5,4,5,5,5
BBUT	Black Butte	244.28019	33.66375	7269	disk in concrete	JPL-CDP/CWU	5,5,5,5,5,5
CEDA	Cedar Creek	241.41227	35.74501	HPGN 0614 1991	rod driven to refusal	Caltrans/CWU	5,5,5,5,5,5
5445	Darwin	241.86784	36.46609	P166-5445	brass cap in rock	USGS/CWU	4,5,3,6,6,13
DEER	Tehachapi	241.49225	35.08576	DEER 1932	brass cap in rock	USGS/CWU	4,6,6,6,5,5
FUNE	Funeral	243.52467	36.39743	3058-S	steel pin in bedrock	JPL/CWU	6,5,5,5,5,3
JOBU	Johannesburg	242.30794	35.33702	Joburg NCER 1973 reset 1977	brass cap in bedrock	USGS/CWU	5,5,5,5,6,5
KMED	Kennedy Meadows	241.86434	36.02325	3187S	steel pin in rock	JPL/CWU	5,4,5,6,6,7
MOJA	Mojave (at Goldstone)	243.10848	35.33124	7288	disk in concrete	JPL-CDP/CWU	5,5,3,6,6,5
MOND	Monday	242.29410	34.74296	MONDAY RS 1929	brass cap in bedrock	USGS-LA Co./CWU	3,4,5,5,5,5
OVRO	Owens Valley Radio Obs.	241.70621	37.23256	7114	rod driven to refusal	JPL-CDP/CWU	4,4,13,5,7,6
PANA	Panamint	242.82566	36.29405	3059-S	steel pin in bedrock	JPL/CWU	4,5,5,6,6,5
RAIN	Rainbow	242.79250	34.97484	RAINBOW	rod driven to refusal	SB Co./CWU	3,5,5,7,4,6
RITA	Santa Rita	241.89897	36.91414	3191S	steel pin in rock	JPL/CWU	7,4,4,5,6,6
RVAL	Round Valley	244.59804	35.14167	3055S	steel pin in rock	JPL/CWU	4,5,5,5,5,5
SCTY	Scotty's Castle	242.86347	37.21820	3260S	steel pin in rock	JPL/UM&CWU	0,6,4,0,0,8
SIBE	Siberia	243.98442	34.62426	3056S	steel pin in bedrock	JPL/CWU	5,5,6,5,6,5
TEAK	Teakettle	242.45354	36.75941	3230S	steel pin in bedrock	JPL/UM	0,5,6,0,0,8
TROY	Troy	243.46946	34.83860	3057S	steel pin in bedrock	JPL/CWU	6,5,6,6,6,5
3188	Wonoga	242.35903	36.30694	3188S	steel pin in bedrock	JPL/CWU	5,5,6,5,5,5
WSTG	Westguard Pass	241.84798	37.27073	3201S	steel pin in bedrock	JPL/CWU & UM	5,5,5,5,5,5

[a]Figures refer to the number of station observation days in each of the years 1993, 1994, 1995, 1996, 1997, and 1998.

during six annual experiments between 1993 and 1998 (Table 1). Most stations were occupied for five 8-24 hour days each year. A subset of the stations had been previously observed from 1991 to early 1993; those results are reported separately [*Miller et al.*, 1993].

2.1. Data Analysis

We performed GPS data analysis with the Jet Propulsion Laboratory (JPL) software package, GPS Inferred Positioning System/Orbit Analysis and Simulation Software (GIPSY/OASIS-II) using fiducial-free global orbit products and a precise point positioning strategy [*Zumberge et al.*, 1997]. Analysis of campaign-mode data consists of several steps: daily solutions derived with weak constraints on initial positions are determined using global orbit products; both the campaign data and continuous stations from the region and from tectonically stable regions of interior North America are included in this analysis. The weakly constrained daily frame is transformed to the International Terrestrial Reference Frame (ITRF96) [*Boucher et al.*, 1998; *Sillard et al.*, 1998] using JPL daily frame files. Daily and seasonal irregularities in the global reference frame are minimized using a regional stabilization [*Bock et al.*, 1997; *Wdowinski et al.*, 1997]. Uncertainty estimates for daily position are scaled such that the ratio of χ^2 to degrees of freedom equals 1. The positions and velocities for each station are combined (Figure 3), and a time-correlated error model is applied to station velocities.

Error estimation strategies built into GIPSY/OASIS-II treat the day-to-day uncertainties in position, which ultimately generate station velocities, as white or temporally uncorrelated noise [*Zumberge et al.*, 1997]. If time-correlated or "colored" noise is present, the velocity uncertainty will be underestimated if pure white noise is assumed [*Johnson and Agnew*, 1995]. Detailed evaluation of error spectra from continuous GPS stations have shown the contribution of both white noise and time-correlated noise [*Zhang et al.*, 1997]. Possible sources of colored noise in GPS include monument motion unrelated to tectonic deformation [*Langbein and Johnson*, 1997], uncertainty in the satellite orbit parameters, and atmospheric and local environmental effects [*Mao et al.*, 1999]. Mao et al. present an empirical model for estimating the GPS rate error σ_r for individual velocity components (north, east, and vertical) for coordinate time series in the presence of combined white and colored noise:

$$\sigma_r^2 \cong \frac{12\sigma_w^2}{gT^3} + \frac{a\sigma_f^2}{g^b T^2} + \frac{\sigma_{rw}^2}{T} \qquad (1)$$

where g is the measurement frequency, T is the total time span of observations (5 years for most stations in this study), a and b are empirical constants (a=1.78 and b=0.22), σ_w is white noise (no time correlation), σ_f is flicker noise (time correlated with spectral power inversely proportional to frequency), and σ_{rw} is random walk noise (depends on monument stability and time span of observations) in mm/$\sqrt{}$yr.

Application of this error model requires estimates for white, flicker, and random walk noise, which depend in part on local station characteristics. Mao et al.'s data show a correlation between the weighted root-mean-square (WRMS) scatter of an individual time series and corresponding magnitudes of white and flicker noise values. *Dixon et al.* [2000] use this relationship to estimate white and colored noise magnitudes for individual GPS time series, where a sufficient number of obser-

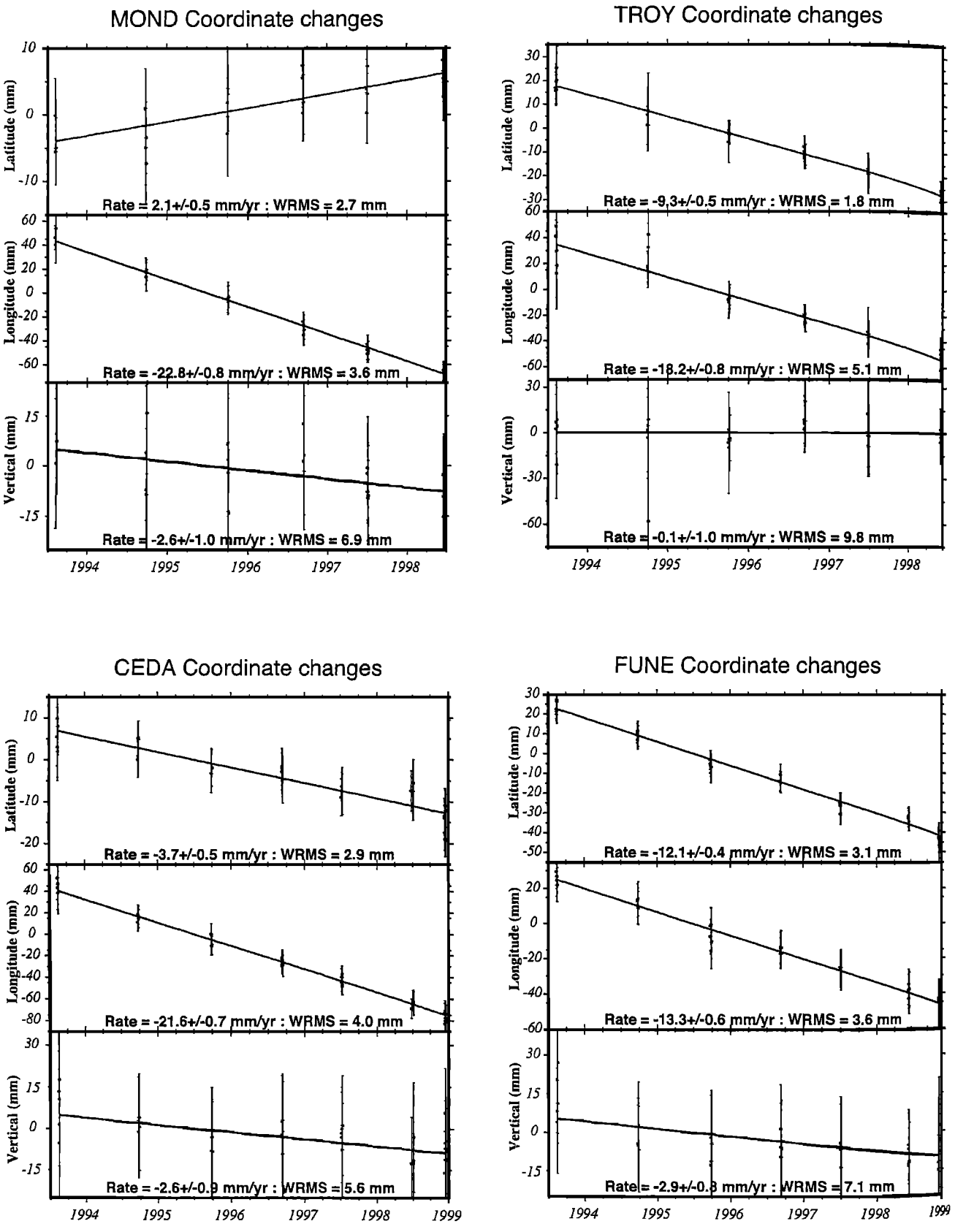

Figure 3. Representative time series for GPS stations within the network. North, east, and vertical components of motion are shown in ITRF96 for stations Monday, Troy, Cedar, and Funeral. A white noise error model (shown here) yields scaling factors for the error model of Mao et al. [1999], which estimate uncertainties due to both time-correlated and white noise (Tables 2 and 3).

vation days are available to ensure that WRMS is an indicator of data quality. We have adopted this approach here.

Station position and velocity are reported here in two reference frames: as station velocities relative to the International Terrestrial Reference Frame (ITRF96) (Table 2 and Figure 3) and relative to North America (Table 3 and Plate 1). In this analysis, North America was defined by 10 GPS stations that lie on the relatively stable continental interior, east of the Rocky Mountain front. This realization is robust; all stations used to define North America show horizontal residuals less than 1.4 mm/yr (Table 3).

2.2. Comparison to Other Data

Stations common to our analysis and the Southern California Earthquake Center (SCEC) velocity field, version 2 [*Shen et al.*, 1998] provide a point of comparison for independent processing techniques. The SCEC data were analyzed using GAMIT/GLOBK software, and the data set includes a different set of observation days. The two solutions have five continuous stations in common (BLYT, CICE, COSO, GOLD, and MATH; see Table 4) and three other marks occupied in survey mode (MOND, MOJA and, BBUT; see Tables 1 and 4). There are some caveats in making this comparison. Stations may have a different number of observations per year in the two analyses (ours are typically 5 days), and the reported time interval of observation is different between the two solutions (Table 4). The SCEC velocities are presented in a North America reference frame defined somewhat differently than our study. Also, the SCEC solution spans the time of the Landers earthquake for all but three of the continuous stations (BLYT,

Table 2. Regional GPS Station Velocities in the International Terrestrial Reference Frame (ITRF96) for 1993-1998.

Station	Longitude, °E	Latitude, °N	E Velocity, mm/yr	N Velocity, mm/yr	E Velocity Error	N Velocity Error	Correlation
ABER	241.71170	36.97906	-19.64	-5.42	2.03	1.18	-0.04263
ALGO	281.92863	45.95580	-15.78	0.63	0.76	0.47	0.03672
BAMA	241.88052	36.60256	-18.92	-4.19	1.50	0.95	-0.17180
BBUT	244.28019	33.66375	-14.93	-9.81	1.52	0.89	-0.14799
BLYT	245.28515	33.61042	-12.84	-11.49	0.46	0.30	0.00345
BRMU	295.30373	32.37040	-12.51	7.61	1.09	0.53	-0.00021
CEDA	241.41227	35.74501	-21.63	-3.68	0.83	0.72	-0.07969
CICE	243.33262	31.87126	-39.36	17.47	0.61	0.36	0.03183
COSO	242.19111	35.98234	-14.20	1.66	0.65	0.37	-0.00093
5445	241.86784	36.46609	-18.95	-5.36	0.90	0.62	-0.07667
DEER	241.49225	35.08576	-21.53	-0.40	0.97	0.94	-0.01201
FAIR	212.50076	64.97800	-7.59	-22.3	0.54	0.55	-0.00581
FUNE	243.52467	36.39743	-13.32	-12.06	0.73	0.77	-0.01687
GODE	283.17317	39.02173	-14.19	2.28	0.88	0.44	0.00766
GOLD	243.11075	35.42516	-16.49	-6.90	0.39	0.30	-0.00035
JOBU	242.30794	35.33702	-19.03	-2.07	0.83	0.70	-0.16184
KMED	241.86434	36.02325	-19.03	-3.34	0.97	0.69	-0.01820
MDO1	255.98501	30.68051	-10.96	-8.17	0.42	0.25	0.00518
MOJA	243.10848	35.33124	-17.06	-6.02	0.61	0.62	-0.03671
MOND	242.29410	34.74296	-22.85	2.09	0.85	0.77	-0.10954
NLIB	268.42511	41.77159	-14.37	-3.83	0.79	0.44	0.05076
OVRO	241.70621	37.23256	-18.63	-7.27	0.94	0.63	0.00294
PANA	242.82566	36.29405	-16.01	-9.02	1.03	0.81	-0.04863
PIE1	251.88107	34.30151	-11.27	-9.99	0.35	0.20	0.01668
PVEP	241.59576	33.74329	-34.71	17.94	0.66	0.47	-0.01979
QUIN	239.05557	39.97455	-19.99	-5.79	0.92	0.69	-0.00197
RAIN	242.79250	34.97484	-18.83	-1.13	0.92	0.55	-0.14976
RITA	241.89897	36.91414	-18.36	-7.19	0.80	0.64	-0.03475
RVAL	244.59804	35.14167	-13.14	-11.71	0.92	0.63	-0.01895
SCTY	242.86347	37.21820	-14.01	-12.26	1.07	0.57	-0.03105
SIBE	243.98442	34.62426	-11.96	-12 79	0.74	0.72	-0.02352
STJO	307.32225	47.59524	-14.61	12.29	0.92	0.55	-0.01788
TEAK	242.45354	36.75941	-14.79	-9.72	0.96	0.99	-0.05120
THU1	291.21200	76.53734	-21.79	3.91	0.59	0.91	-0.02606
TROY	243.46946	34.83860	-18.25	-9.33	1.19	0.51	-0.10222
VNDP	239.38355	34.55631	-40.14	20.83	0.44	0.34	-0.02366
WES2	288.50668	42.61334	-14.82	3.36	0.95	0.57	0.04449
3188	242.35903	36.30694	-16.39	-8.66	1.27	0.72	-0.12933
WSTG	241.84798	37.27073	-17.96	-8.15	0.76	0.52	-0.03258
YELL	245.51930	62.48089	-16.13	-11.92	0.42	0.47	-0.02568

Table 3. Regional Station Velocities Relative to North America, 1993-1998, Determined by GPS Sites on Stable North America.

Station	Longitude, °E	Latitude, °N	E Velocity, mm/yr	N Velocity, mm/yr	E Velocity Error, mm/yr	N Velocity Error, mm/yr	Correlation
			Stations Defining North America				
ALGO	281.93	45.96	0.32	-0.95	0.78	0.50	0.0323
BRMU	295.30	32.37	-1.04	0.89	1.11	0.57	0.0272
GODE	283.17	39.02	-0.12	0.26	0.90	0.47	0.0182
MDO1	255.99	30.68	-0.40	0.24	0.48	0.28	-0.0195
NLIB	268.43	41.77	0.35	-0.06	0.81	0.46	0.0491
PIE1	251.88	34.30	0.05	-0.08	0.41	0.24	-0.0260
STJO	307.32	47.60	-0.14	1.25	0.94	0.60	-0.0037
THU1	291.21	76.54	-0.47	-1.26	0.64	0.93	-0.0717
WES2	288.51	42.61	0.15	-0.72	0.97	0.60	0.0475
YELL	245.52	62.48	0.74	0.20	0.46	0.49	0.0300
			Regional GPS Network Stations				
3188	241.87	36.47	-8.23	7.89	0.92	0.64	-0.0832
5445	242.36	36.31	-5.61	4.43	1.29	0.74	-0.1312
ABER	241.71	36.98	-8.74	7.89	2.04	1.29	-0.0442
BAMA	241.88	36.60	-8.10	9.08	1.51	0.96	-0.1720
BBUT	244.28	33.66	-4.57	2.71	1.54	0.90	-0.1496
BLYT	245.29	33.61	-2.36	0.68	0.51	0.34	-0.0380
CEDA	241.41	35.75	-11.08	9.73	0.86	0.74	-0.0868
CICE	243.33	31.87	-29.67	30.32	0.65	0.39	-0.0088
COSO	242.19	35.98	-3.52	14.88	0.68	0.41	-0.0253
DEER	241.49	35.09	-11.14	13.01	0.99	0.95	-0.0198
FAIR	212.50	64.98	0.85	-1.79	0.56	0.61	0.0332
FUNE	243.52	36.40	-2.33	0.66	0.76	0.79	-0.0257
GOLD	243.11	35.43	-5.84	5.99	0.44	0.34	-0.0450
JOBU	242.31	35.34	-8.47	11.05	0.86	0.72	-0.1643
KMED	241.86	36.02	-8.35	9.99	0.99	0.71	-0.0271
MATH	242.56	33.86	-22.92	25.57	0.38	0.28	-0.0945
MOJA	243.11	35.33	-6.46	6.89	0.65	0.64	-0.0501
MOND	242.29	34.74	-12.53	15.25	0.88	0.79	-0.1150
OVRO	241.71	37.23	-7.66	6.04	0.96	0.65	-0.0068
PANA	242.83	36.29	-5.15	3.98	1.05	0.83	-0.0539
PVEP	241.60	33.74	-24.68	31.27	0.70	0.50	-0.0430
QUIN	239.06	39.97	-8.79	8.36	0.94	0.71	-0.0090
RAIN	242.79	34.97	-8.30	11.89	0.94	0.57	-0.1533
RITA	241.90	36.91	-7.52	6.08	0.83	0.66	-0.0439
RVAL	244.60	35.14	-2.32	0.70	0.94	0.65	-0.0282
SCTY	242.86	37.22	-2.90	0.67	1.09	0.59	-0.0379
SIBE	243.98	34.62	-1.44	-0.19	0.77	0.74	-0.0343
TEAK	242.45	36.76	-3.88	3.40	0.98	1.00	-0.0555
TROY	243.47	34.84	-7.75	3.47	1.21	0.54	-0.1069
VNDP	239.38	34.56	-30.17	34.86	0.49	0.38	-0.0685
WSTG	241.85	37.27	-7.03	5.09	0.79	0.55	-0.0437

CICE, and COSO). Detectable coseismic offsets for Landers were determined at Monday (MOND), Mojave (MOJA), and Black Butte (BBUT); in the SCEC solution these offsets would contribute to annual velocities except where a separate, post-Landers earthquake velocity (annotated "_cLA", Table 4) is indicated.

Despite these caveats the data generally agree within uncertainties (Table 4). In particular, for stations within the Mojave block the north velocities agree to better than 1 mm/yr, with our velocities slightly but systematically higher than the SCEC solution. For the east component, agreement is within 1.5 to 2 mm/yr and generally within uncertainty estimates. The exception is Mojave (MOJA), where agreement is worse. The discrepancy may be due to the fact that the observations in the SCEC solution span the time of the Landers earthquake without a coseismic correction (Table 4). In addition, fewer recent data are included there, and post-1992 analyses are generally more robust. There are two common stations where the Landers earthquake displacement is accounted for in the SCEC solution, one survey mode and one continuous (GOLD and MOND; see Table 4); the agreement is not particularly good, but the SCEC solution includes 1992 data which could be biased by short-term postseismic deformation. While our error estimates are somewhat lower, particularly in the north component, this is consistent with a greater number of annual observations and, in some cases, a greater number of years in our solution. In summary, apart from effects potentially related to time-variant deformation from the Landers earthquake, the two solutions agree within one standard error.

3. Results

3.1. GPS Velocity Field

The velocity results (Plate 1) indicate that motion of ~ 2 mm/yr relative to stable North America occurs east of our GPS network. Part of this may result from strain accumulation on faults to the west, including faults composing the shear zone

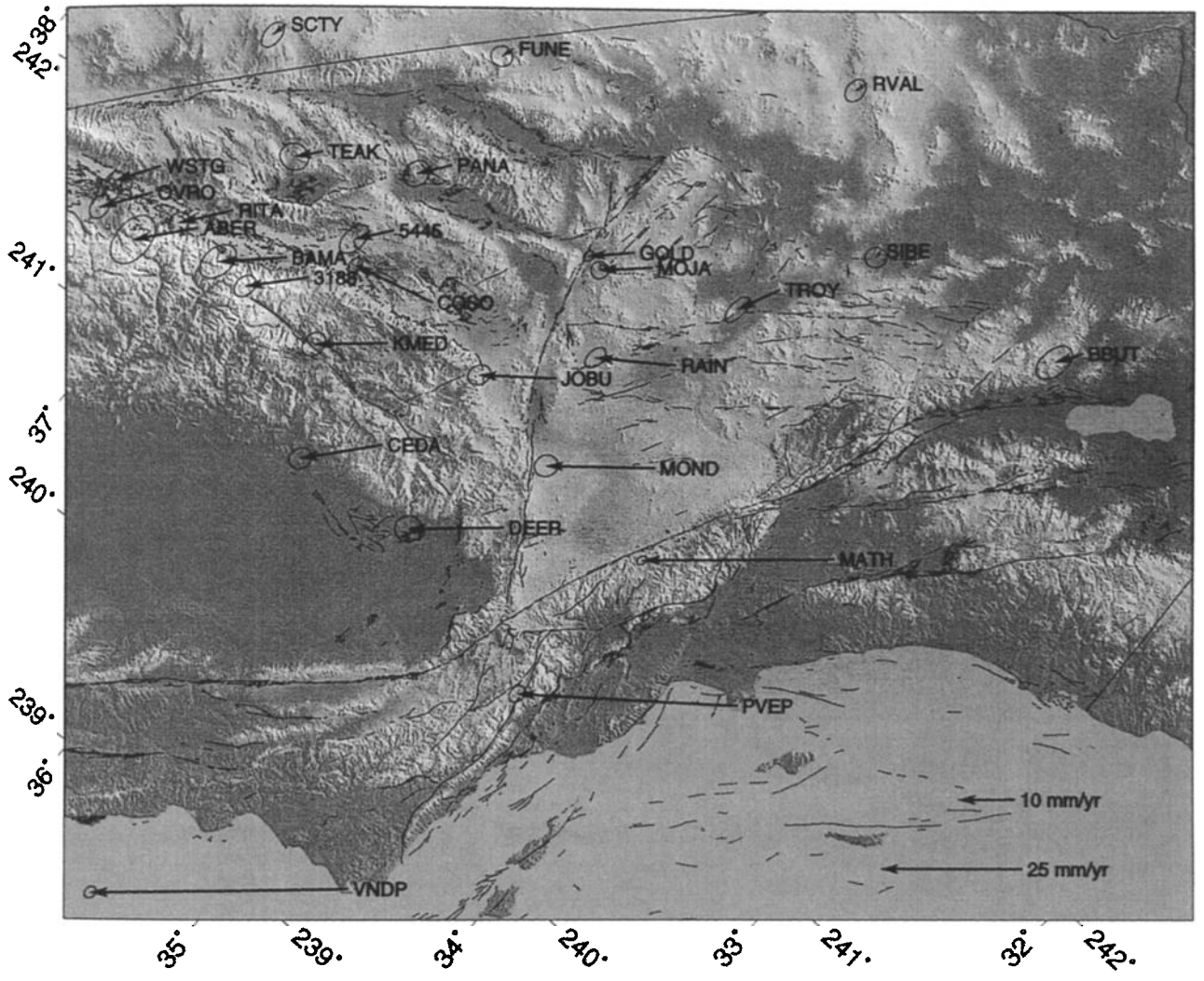

Plate 1. GPS-determined velocity field, Eastern California shear zone, 1993–1998. Velocity field is relative to nominal North America, where North America is defined by 10 stations that are analyzed in common with the regional network solution in ITRF96, which lie east of all Cordilleran deformation (Table 3). Error ellipses show two-dimensional 95% confidence. Station velocities are given in Table 3. The velocities are plotted on an oblique Mercator projection parallel to the Pacific–North America relative plate motion direction determined by DeMets and Dixon [1999]. Predicted Pacific–North America motion is thus parallel to the edge of the map oriented N41°W at the latitude of the Mojave segment of the San Andreas fault. Fault map is from Jennings [1994]. The Landers and Hector Mines surface ruptures are plotted in red. Shaded topographic relief and projection were calculated from U.S. Geological Survey 1:250,000 digital elevation models using GMT [*Wessel and Smith*, 1995].

Table 4. Comparison Between the Results of this Study and the SCEC Horizontal Deformation Velocity Map Version 2.0.

GPS Station[a]	Longitude, °E	Latitude, °N	East Velocity, mm/yr	North Velocity, mm/yr	East σ, mm/yr	North σ, mm/yr	Correlation Coefficient	Years observed	Coseismic Landers earthquake offset[b] in mm	
									East	North
Black Butte										
BLAC_GPS	244.28010	33.66380	-3.11	1.37	0.62	0.58	-0.0397	1988, 1990-1995, 1997		
BBUT	244.28	33.66	-4.57	2.71	1.54	0.90	-0.1496	1993-1998	42.9±15.2	-4.0±4.4
Blythe										
BLYT_GPS	245.28504	33.61049	-1.40	-0.14	0.55	0.51	-0.0271	1994-1997 continuous		
BLYT	245.29	33.61	-2.36	0.68	0.51	0.34	-0.0380	1994-1998 continuous		
Cicese										
CICE_GPS	243.33262	31.87126	-30.57	30.16	0.68	0.65	0.0028	1995-1997 continuous		
CICE	243.33	31.87	-29.67	30.32	0.65	0.39	-0.0088	1995-1998 continuous		
Coso Geothermal field										
COSO_GPS	242.19111	35.98234	-2.90	14.41	0.76	0.73	0.0323	1995-1997 continuous		
COSO	242.19	35.98	-3.52	14.88	0.68	0.41	-0.0253	1995-1998 continuous		
Goldstone										
GOLD_GPS	243.11081	35.42503	-3.02	6.73	0.78	0.65	0.0020	1987-1992 continuous		
GOLD_cLA	243.11081	35.42503	-7.54	5.53	0.51	0.47	-0.0220	1992-1997 continuous		
GOLD	243.11	35.43	-5.84	5.99	0.44	0.34	-0.0450	1993-1998 continuous	-5.0±2.0	-11.0±1.0
Lake Matthews										
MATH_GPS	242.56350	33.85630	-23.98	25.54	0.55	0.52	-0.0181	1992-1997 continuous		
MATH	242.56	33.86	-22.92	25.57	0.38	0.28	-0.0945	1993-1998 continuous		
Monday										
MDAY_GPS	242.29423	34.74280	-11.41	17.30	1.89	1.25	-0.1377	1988,1990		
MDAY_cLA	242.29423	34.74280	-16.14	13.62	1.60	1.28	-0.0184	1992-1995		
MOND	242.29	34.74	-12.53	15.25	0.88	0.79	-0.1150	1993-1998	-16.6±12.8	40.7±3.7
Mojave										
MOJM_GPS	243.11190	35.33139	-2.44	8.59	0.72	0.61	-0.0102	1989-1992		
MOJA	243.11	35.33	-6.46	6.89	0.65	0.64	-0.0501	1993-1998	-5.0±2.0	-11.0±1.0

[a] Sations ending in "_GPS" are the GAMIT solution from *Shen et al.* [1998]; "_cLA" indicates a solution that only includes data from after the 1992 Landers earthquake; in these cases the "_GPS" is a solution from data collected prior to the Landers; four-character identifications give GIPSY 1993-1998 solutions presented in this paper.

[b] From *Miller et al.* [1993].

and even the San Andreas fault. This is evaluated by an elastic strain accumulation model, discussed below. Within the Eastern California shear zone, the distribution of slip is broadly continuous at a plate boundary scale (Plate 1 and Figure 4); on a regional scale, however, the dominance of specific fault zones in the total slip budget is apparent (Plate 1 and Figure 4). The anomalous velocity at the Coso geothermal field (COSO) is likely related to the local geothermal sources or geothermal production. Our data do not resolve slip rates on each of the 30 or more fault segments that are active in eastern California. Rather, they illuminate the loci of deformation in various structural domains, provide constraints on the total slip budget, and yield slip rate estimates for some specific major faults.

Immediately north of the Salton Sea, deformation is concentrated along the San Andreas fault and Borderland faults to the west. Plate margin related dextral shear penetrates the southern Mojave Desert block, broadening the zone of continental deformation at the plate boundary east of the San Andreas fault (Plate 1). The zone of deformation becomes wider

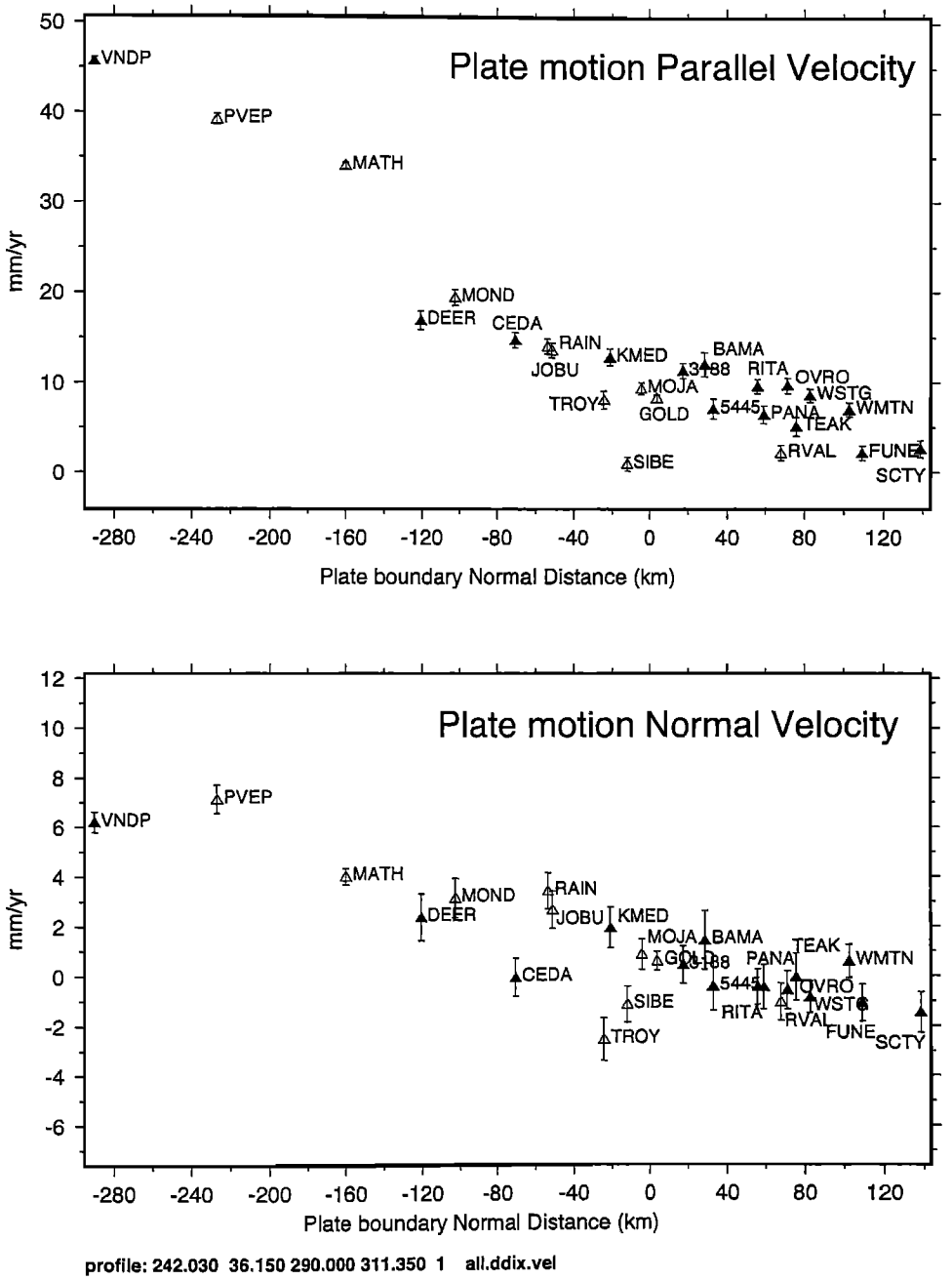

Figure 4. Plate motion parallel and normal components of regional GPS station velocities. This profile decomposes station velocities parallel and perpendicular to Pacific–North America plate motion [DeMets and Dixon, 1999] and plots them against distance from an arbitrary origin near the center of the Eastern California shear zone. Solid symbols are stations north of the Garlock fault; open symbols are stations to the south. For plate motion normal velocities, a positive slope between any two stations implies extension, and a negative slope implies extension.

and penetrates the continent as the Eastern California shear zone crosses the Mojave Desert block. South of Barstow, the deformation occurs in the western part of the zone, along the Calico-Blackwater fault, and faults farther west. North of Barstow, the shear zone becomes wider, resulting in deformation in the northeastern Mojave block that feeds about half of the Eastern California shear zone slip onto the Panamint-Hunter Mountain and Death Valley-Fish Lake Valley fault zones.

3.2. Relationship to Plate Motion Direction

Station velocities are resolved onto plate motion parallel and plate motion perpendicular components in Figure 4. Stations both north and south of the Garlock fault show that dextral shear is distributed over several hundreds of kilometers of the continental plate margin. For stations south of and near the Garlock fault, deformation is concentrated nearer the San Andreas fault (Figure 4), and station Monday (MOND, Plate 1) is close enough to the Mojave segment of the San Andreas fault to be strongly entrained in its elastic deformation field. In contrast, dextral deformation of stations north of the Garlock fault or near its eastern end is concentrated somewhat farther to the northeast and away from the San Andreas fault. This shift in the locus of deformation away from the San Andreas fault is also apparent in the plate motion normal component of deformation (Figure 4). The faults comprising the Eastern California shear zone strike more northerly than the plate motion direction, thus extension is a consequence of the northwest oblique motion on north to north-northwest striking faults (Plate 1).

These patterns are not surprising in light of the extent and coherence of the Sierra Nevada as a structural block [*Dixon et al.*, 2000] and the inland penetration of the shear zone [*Wallace*, 1984; *Bennett et al.*, 1997; *Thatcher et al.*, 1999; *Dixon et al.*, 2000; *Gan et al.*, 2000]. They point to the role of sinistral motion on the Garlock fault in accommodating different styles of deformation oblique to Pacific–North America motion in adjacent structural domains.

3.3. Relating GPS Velocities to Estimates of Long-Term Deformation

GPS velocities average over several years, but we would like to compare these data to longer-term averages, in particular, the geologic slip rate on faults. This requires a mechanical model that accounts for elastic strain accumulation on locked or partly locked faults. In a complex region like the one under discussion, with 30 or more active fault segments slipping at various rates and with potentially different locking depths, this is not a tractable problem using current geodetic data sets. If all the parameters were treated as unknowns (fault geometry, locking depth and slip rate), there would be hundreds of variables and only ~ 50 data to constrain the problem.

Our approach is to constrain the fault geometry, including effective locking depth, on all faults in the region from other available information and to constrain fault slip rates where known from other sources (Table 5). We then use our relatively sparse but regionally synoptic data to estimate unknown slip rates on a few key fault segments via forward modeling (Figure 5). We use the three-dimensional elastic deformation code 3D-DEF [*Gomberg and Ellis*, 1994] as it allows us to incorporate the complex fault geometry and fault segmentation that are critical features of this portion of the Eastern California shear zone. We have digitized fault segments from *Jennings* [1994] and adopted the San Andreas fault locking constraints of *Feigl et al.* [1993]. In places where stations are too sparse to resolve multiple fault segments and geodetic constraints are sparse we have simplified known fault geometry (Figure 5).

The effective depth of coupling [*Savage and Lisowski*, 1998] and the Holocene slip rate (34 mm/yr) [*Sieh and Jahns*, 1984; *Weldon and Sieh*, 1985; *Sieh et al.*, 1989] on the San Andreas fault are relatively well known and large. Thus the effects of elastic coupling at the millimeter per year level are evident several hundred kilometers from the San Andreas fault. This implies discernible entrainment of most of the width of southern California in the elastic deformation field of the San Andreas fault. Relatively shallower effective locking depths for the southern San Andreas fault, near the Salton Sea, minimizes this effect south of the Mojave Desert block (Plate 1). The correction for the San Andreas fault elastic effect primarily affects station velocities in the western part of our network as well as the total budget for Eastern California shear zone deformation. For all other faults we assume a locking depth of 10 km and use slip rates determined from fitting GPS results in profiles across each fault.

In the model, slip on each of the fault segments is driven at depth to proxy long-term deformation. The model predicts the integrated deformation at any given set of points, in this case at the location of the GPS stations. Estimates of the interseismic elastic strain accumulation and geologic rates of slip are differenced with the GPS velocities, yielding a residual at each station. This residual potentially includes contributions from a variety of sources: any mismodeling of long-term deformation rates on known fault segments, model neglect of block rotations, earthquake postseismic deformation from Landers and other earthquakes, mismodeled elastic deformation fields, and differences between the simple elastic model shown here and more realistic rheology.

The response of the lower crust and upper mantle to the earthquake cycle potentially has a significant impact on the surface velocity field. At least in the case of two stations within 50 km of the Landers surface rupture (TROY, SIBE), postseismic effects are notable relative to uncertainties in GPS velocities (the observation interval here ends before the 1999 Hector Mine earthquake). SCEC reports a spatially dense data set aimed at characterizing post-Landers earthquake time-variant deformation [*Wdowinski et al.*, 1997] to the south of our study area.

We can account for some earthquake cycle effects by varying the locking depth of the elastic half space model to an appropriate value (e.g., deeper locking depth for faults late in their earthquake cycle [*Savage and Lisowski*, 1998]).

4. Discussion

Geological, geophysical, and geodetic data collectively point to the kinematic importance of the Eastern California shear zone in accommodating Pacific–North America plate motion. The GPS constraints presented here reveal first-order refinements to our understanding of the role of the Eastern California shear zone: (1) The total fault slip budget within our network, while variable along strike, is greater than in some previous reports. (2) The motion of some stations relative to

Table 5. Model Faults.

Fault segment				Locking Depth, km	Slip Rate, mm/yr	
Longitude, °E	Latitude, °N	Longitude, °E	Latitude, °N		Sinistral Strike Slip	Opening
			San Andreas and Related Faults			
240.600	34.950	"infinite"	(318°)	-25	-34.5	-3.0
240.600	34.950	241.545	34.680	-25	-34.2[a]	0.0[a]
241.545	34.680	242.525	34.280	-12	-27.2[a]	0.0[a]
242.525	34.280	243.800	33.800	-7	-15.4[a]	0.0[a]
243.800	33.800	245.000	32.930	-5	-29.2	-4.5
245.000	32.930	"infinite"	(138°)	-5	-29.5	0.0
242.525	34.280	"infinite"	(274°)	-10	0.0	-6.5
242.525	34.280	242.940	33.830	-10	-12.0	0.3
242.940	33.830	"infinite"	(138°)	-10	-12.0	0.0
			Owens Valley Fault			
242.100	35.880	241.500	38.080	-10	-7.0	2.0
242.240	35.420	242.100	35.880	-10	-7.0[a]	0.0[a]
			Hunter Mountain and Related Faults			
242.100	37.500	241.900	37.100	-10	1.4[a]	0.0[a]
241.900	37.120	242.200	36.700	-10	0.0	2.0
242.200	36.700	242.600	36.480	-10	-1.7	0.0
242.600	36.480	243.000	35.600	-10	-2.7[a]	0.0[a]
			Death Valley and related Faults			
241.500	38.080	"infinite"(318°)		-10	-13.0	5.0
241.500	38.080	242.100	37.500	-10	-5.0	3.0
242.100	37.500	243.250	36.530	-10	-5.0	3.0
243.250	36.530	243.320	35.880	-10	-4.7[a]	0.0[a]
243.320	35.880	243.350	35.600	-10	-5.0	3.0
243.320	35.880	243.630	35.600	-10	-3.8[a]	0.0[a]
			Garlock Fault			
241.065	34.820	242.240	35.420	-10	5.0	-1.0
242.240	35.420	243.000	35.600	-10	5.0	0.0
243.000	35.600	243.350	35.600	-10	2.5	0.0
243.350	35.600	243.630	35.600	-10	1.1[a]	0.0[a]
			Faults of the Mojave Desert			
243.800	33.800	242.050	35.350	-10	-4.0	0.3
242.580	35.550	242.990	35.050	-10	-5.5	0.0
242.990	35.050	243.500	34.500	-10	-8.0	0.0
242.840	35.600	243.200	35.100	-10	-2.0	0.0
243.200	35.100	243.500	34.500	-10	-1.8	0.3
243.350	35.600	243.700	35.150	-10	-5.0	3.0
243.700	35.150	243.800	33.800	-10	-2.5	2.6
243.630	35.600	243.940	35.150	-10	-3.0	3.0
243.700	35.150	243.200	35.100	-10	2.5	8.0
243.940	35.150	243.700	35.150	-10	0.0	4.0
243.500	34.500	243.800	33.800	-10	-9.6	2.7

[a]No initial constraint put into model.

stable North America in the eastern part of the network refines our understanding of plate margin distributed deformation and reconciles earlier discrepancies in interpretations. (3) The kinematic consequences of these results imply a larger seismic moment budget for the Eastern California shear zone than previously determined.

Our results indicate a total slip budget for the Eastern California shear zone of ~14 mm/yr within the Mojave Desert block and 13 mm/yr between the eastern flank of Death Valley and the western flank of the Sierra Nevada, north of the Garlock fault, when San Andreas-related elastic deformation is taken into account [e.g., *Feigl et al.*, 1993; *Savage and Lisowski*, 1998]. This latter estimate agrees with the 11.4 mm/yr of total right-lateral slip estimated by *Dixon et al.* [2000] in a transect across northern Owens Valley, north of the network described here. The 1-2 mm/yr of motion east of the network (e.g., motion of FUNE, SCTY, and RVAL; Plate 1 and Figure 4 and 5) does not necessarily indicate additional active faulting immediately east of these stations. Rather, it represents the sum of elastic strain accumulation effects from the San Andreas fault and faults composing the Eastern California shear zone as well as the cumulative effect of east-west extension in the Basin and Range on faults such as the Wasatch fault [*Thatcher et al.*, 1999; *Dixon et al.*, 2000]. Thus our data combined with an elastic strain model do not allow for significant (greater than ~ 1 mm/yr) right lateral shear east of Death Valley in the southern Basin and Range.

4.1. Pattern and Magnitude of Deformation Within the Mojave Desert Block

The triangular Mojave Desert block is defined by the San Andreas fault to the southeast and the Garlock fault to the north (Plate 1 and Figure 6); its eastern limit is defined by the southeast trending structural grain of the Avawatz Mountains [*Dokka*, 1986]. It is transected by northwest striking dextral

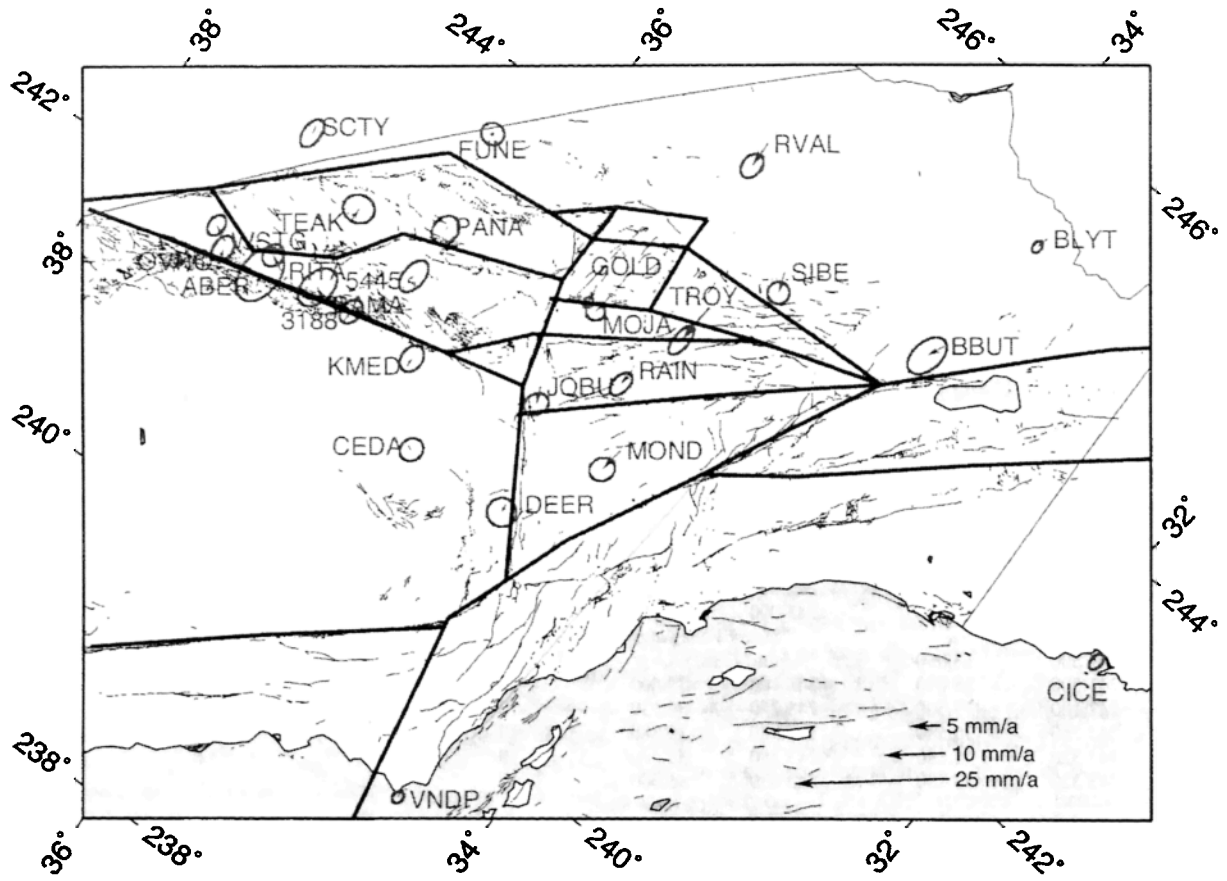

Figure 5. Residual station motions for the elastic dislocation model. Model fault segments are shown in thick lines, residual motions with GPS error are indicated by vectors. Slip rates and fault segments are detailed in Table 5. The residual field indicates good fit of the model, except in the Mojave Desert block south of the Garlock fault. There a small but systematic counterclockwise rotation of residuals on the Mojave block is evident. This rotation indicates mismodeling, which may be attributable to a number of causes: The elastic dislocation model does not allow for block rotations, and thus any longterm Mojave block rotation is neglected in the model and will influence the residual velocity field. Alternatively, rotations may be partly attributable to any mismodeling of the San Andreas fault, which is the major contributor to elastic strain gradients across the region. Third, some of the residual motion is ascribed to postseismic viscoelastic deformation related to the 1992 Landers earthquake.

faults that splinter the upper crust, except perhaps south of the Pinto Mountain fault and in the Northeast Mojave Domain (Figure 6), where westerly striking sinistral faults interact with northwest striking dextral faults and predominantly clockwise vertical axis rotations are thought to play an important role in modern deformation [*Dokka and Travis*, 1990a; *Schermer et al.*, 1996; *Spotila and Sieh*, 2000]. Faults within the Mojave Desert block accommodate a significant Neogene translation and heterogeneous rotation related to plate margin shear, although differing mechanical models have been invoked to describe these motions [*Garfunkel*, 1974; *Luyendyk et al.*, 1980; *Dokka*, 1989; *Dokka et al.*, 1998]. Two main classes of models include through-going shear along contemporaneous faults [*Garfunkel*, 1974; *Luyendyk et al.*, 1980] and westward migrating heterogeneous shear on the predominant dextral faults [*Dokka and Travis*, 1990a]. Geologic offset of 9.6 km occurs on the Calico fault and another 6.4-14.4 km occurs along the Pisgah fault [*Dokka*, 1983; *Dokka and Travis*, 1990a; *Dokka et al.*, 1998]. Strain rate analyses based on Landers earthquake aftershocks also indicate concentration of short term strain in the central Mojave Desert block [*Unruh et al.*, 1996]. On a more local scale the west striking sinistral faults near Fort Irwin have accommodated clockwise rotations [*MacConnell et al.*, 1994; *Schermer et al.*, 1996]; similar deformation may have occurred near the southern edge of the Mojave block [*Luyendyk et al.*, 1980; *Dokka*, 1993; *Dokka et al.*, 1998].

Very shallow locking of the southern San Andreas fault has long been recognized [*Feigl et al.*, 1993]; the low velocity at Black Butte is due to San Andreas coupling (BBUT, Plate 1 and Figure 5), and this pattern is consistent with other GPS results from the Salton trough region [*Bennett et al.*, 1996; *Shen et al.*, 1998]. These observations support the notion that the Eastern California shear zone splays from the San Andreas system north of the Salton Sea. Modern deformation is localized within the southern and central Mojave Desert block (region of the Calico and/or Pisgah faults), and deformation splays near the Northeast Mojave Domain, where significant parts of slip budget feed around or through this domain as well as across the central Garlock fault (Figures 5 and 6).

Geologic offsets combined with slip rate estimates from geodesy imply that the Eastern California shear zone has been active over 10 Myr or longer. *Du and Aydin*, [1996] have ar-

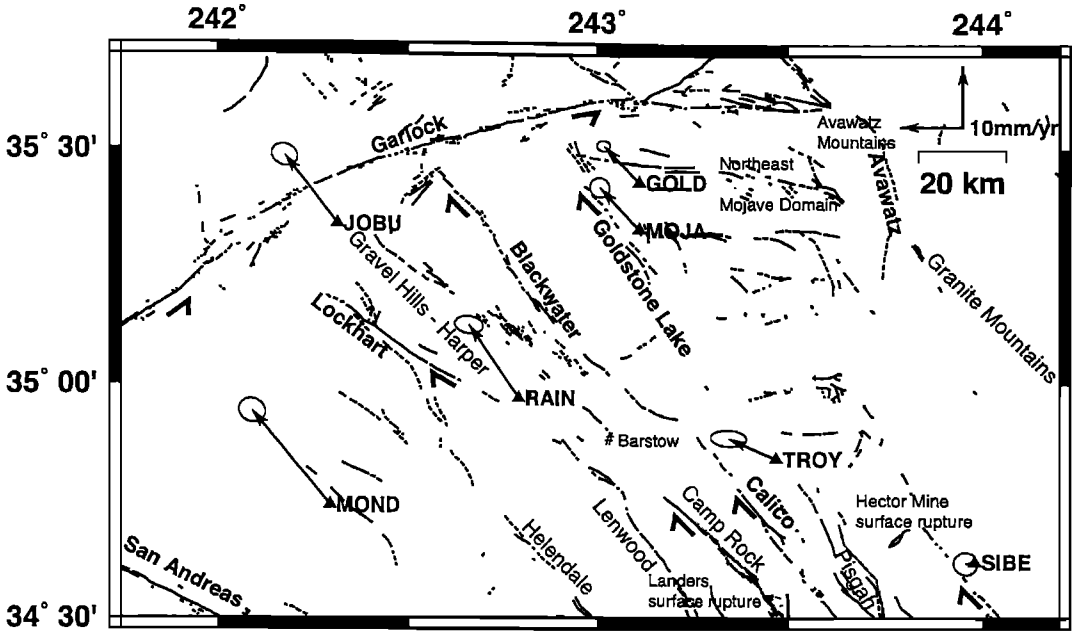

Figure 6. Detail of faults south of the Garlock fault. Fault names are in bold, other features in plain font. GPS station velocities are shown relative to North America (Table 3). Error ellipses show two-dimensional 95% confidence.

gued for the extreme youthfulness of the Eastern California shear zone. Their study misquotes age constraints by an order of magnitude in calculating an Eastern California shear zone age of 0.2-0.4 Ma [see *Rubin and Sieh*, 1997]; the implied minimum ages are actually 2-4 Ma.

On the basis of trilateration the Eastern California shear zone through the central Mojave block has been thought to accommodate ~12 mm/yr [*Sauber et al.*, 1994]; we revise this to 14 mm/yr, based on GPS observations combined with the dislocation modeling. Farther north, most of the Mojave Desert dextral shear had been inferred to step east of Goldstone and Mojave (GOLD and MOJA, Plate 1) because 9 mm/yr directed to the northwest with respect to North America [*Ward*, 1990] was known from very long baseline interferometry (VLBI) observations at the VLBI station Mojave (located at MOJA, Plate 1). This is consistent with the 50% decrease in shear strain between the Mojave and Barstow trilateration networks [*King*, 1985]. Our GPS results show that Goldstone and Mojave are respectively moving 8.4±0.6 and 9.4±0.9 mm/yr to the northwest relative to North America. The combined effects of San Andreas fault interseismic strain accumulation that lies to the east of Mojave and Goldstone and the small budget of northwest-directed motion along faults that lie to east of the Eastern California shear zone as a whole account for ~1-2 mm/year of this velocity relative to North America. Deformation near Goldstone and Fort Irwin feeds ~6-7 mm/yr of fault slip northward across the Garlock fault into the Death Valley region, although details of the partitioning onto northwest striking dextral faults and east-west striking sinistral faults remain to be resolved. In addition, the total budget for the Eastern California shear zone is now larger because the regionally synoptic view presented here indicates significant slip lies farther to the west.

The new GPS data confirm that south of Barstow, much of the modern deformation is localized in the central part of the Eastern California shear zone, consistent with the geologic evidence that half of the Neogene offset is confined to the Calico-Blackwater and Pisgah faults [*Dokka and Travis*, 1990a]. Our network alone is not dense enough to discriminate the role of each fault. On the basis of the motion of Troy and Siberia, which lie 25 and 40 km from the Landers surface rupture (TROY and SIBE, Plate 1 and Figure 7), it is likely that postseismic deformation due to the 1992 Landers earthquake contaminates the velocities of some stations during the 1993-1998 period reported here compared to longer-term averages. Time series from these stations show no significant systematic decay in rates over the five year observation period, consistent with long-term observations elsewhere in California indicating postseismic relaxation times on the order of 20-30 years [*Thatcher*, 1983; *Kenner and Segall*, 2000].

Paleoseismic studies show that the Holocene slip rate of the Emerson fault (southern extension of the Landers surface rupture, Figure 6) relative to the modern slip budget for the Eastern California shear zone is comparable to the ratio of total slip on the Emerson fault relative to the total slip budget of the Eastern California shear zone [*Rubin and Sieh*, 1997]. If this pattern holds for the belt as a whole, then slip rates may be proportional to total offset along each fault [*Dokka and Travis*, 1990a]. The Granite Mountains fault is excluded from the calculation, as geologic [*Dokka and Travis*, 1990a] and geodetic data (this study) indicate that it is no longer active. In this view, roughly 50% of the modern slip budget for the Eastern California shear zone occurs on or near the Pisgah-Rodman and Calico-Blackwater faults in the central Mojave Desert block. The recurrence interval for the Landers event is ~10,000 years along the faults which ruptured [*Rockwell et al.*, 1993; *Rubin and Sieh*, 1997].

Within the Mojave segment of the Eastern California shear zone as a whole, such events must occur more frequently, for example, the Hector Mine earthquake [*Scientists from the U.S. Geological Survey*, 2000]. If all accumulated slip is released coseismically and if 25% of total slip is accommodated on the

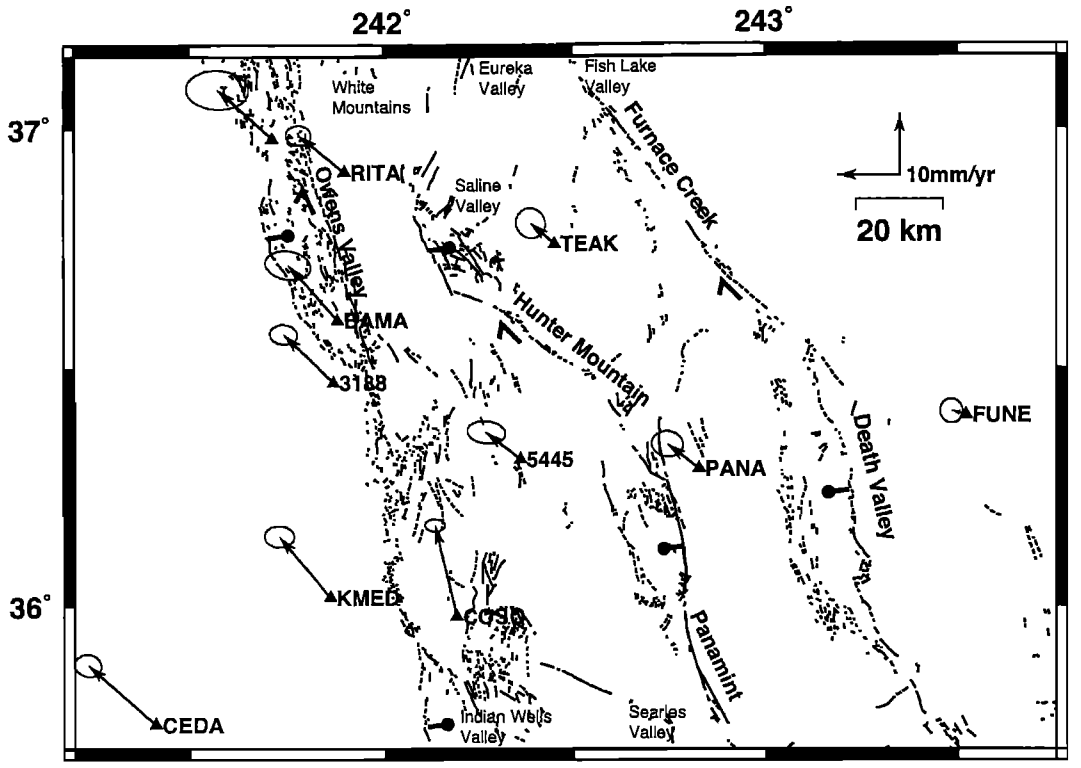

Figure 7. Detail of faults north of the Garlock fault. Fault names are in bold; other features are in plain font. GPS station velocities are shown relative to North America (Table 3). Error ellipses show two-dimensional 95% confidence.

Pisgah-Rodman and Calico-Blackwater faults, then on average, a 4 m surface rupture will occur on each fault every 1100 years. Farther north, within the Northeast Mojave domain, our data suggest that significant deformation steps to the east near the Avawatz Mountains (Figure 6). The Blackwater fault, the northern extension of the Calico fault, and nearby faults are also active (Table 5) at rates of ~7-8 mm/yr. Geologic and paleomagnetic results from the Northeast Mojave domain indicate conjugate fault sets and clockwise paleomagnetic rotations [*MacConnell et al.*, 1994; *Schermer et al.*, 1996]. While we are continuing detailed observations in this region to resolve issues of local GPS station and tectonic stability, the data presented here give a robust post-Landers earthquake estimate of motion between Mojave and Goldstone (MOJA and GOLD, Plate 1) that indicates little resolvable motion between the stations.

Our GPS velocities are consistent with early VLBI data from the GPS station Mojave (MOJA, Plate 1), which showed ~9 mm/yr motion relative to stable North America [*Ward*, 1990]. Approximately 1-2 mm/yr of this motion are attributable to San Andreas entrainment and deformation to the east of the network; thus only 6-7 mm/yr of long term motion passes east of Mojave within the Eastern California shear zone. As much as 7 mm/year passes across the central part of the Garlock fault. This differs somewhat from recent kinematic models that rely on sparse geodetic data [*Hearn and Humphreys*, 1998].

The estimates of velocity and the coherent northwestward motion of the network with respect to North America shed some light on two important relations: block rotations at the eastern end of the Garlock fault and partitioning of Eastern California shear zone slip as it passes northward across the Garlock fault.

4.2. Garlock Fault

The importance of the Garlock fault and its large total offset are well established [*Davis and Burchfiel*, 1973; *Monastero et al.*, 1997]. On the basis of seismicity and fault geometry the Garlock fault has two segments: a western 150 km segment that has microseismicity and appears to be creeping as well as a 115 km eastern segment which is apparently locked; both segments show seismic moment deficit and are thought to pose seismic risk [*Astiz and Allen*, 1983]. In addition, large prehistoric earthquakes are now well documented along the fault [*McGill and Sieh*, 1991, 1993; *McGill and Rockwell*, 1998]. The Garlock fault has 64 km of total geologic offset, and the youngest known rocks that show the total offset are 17 Ma [*Monastero et al.*, 1997]. These geologic relations yield a minimum average slip rate of the Garlock fault over the 17 Ma interval of 3.8 mm/yr; if the initiation of Garlock faulting is younger, the slip rate is higher. Paleoseismic studies prefer 5-7 mm/yr sinistral motion along the length of the fault, although a range of 4-9 mm/yr is permitted [*McGill and Sieh*, 1993; *McGill and Rockwell*, 1998]. If the higher preferred slip rate of 7 mm/yr, determined from paleoseismology, is also the long-term average slip rate, 9 Myr. are required to account for the total geologic offset along the fault. This age is consistent with local stratigraphic constraints on fault initiation from the central Garlock fault [*Burbank and Whistler*, 1987; *Loomis and Burbank*, 1988].

The geometry of our network does not resolve Garlock fault motions in detail but does provide some constraints. In contrast to the relatively fast slip rate implied by geologic relations (3.8 mm/yr minimum, 7 mm/yr if estimates of fault initiation are correct) and paleoseismic results (5-7 mm/yr), GPS

baselines that cross the Garlock fault suggest very low sinistral slip, of the order of 1-2 mm/yr (see misfit in Figure 5, which uses higher geologic rates). Part of the discrepancy could reflect the fact that the Garlock fault may be in the late stages of its earthquake cycle, although estimates vary. The best evidence for recurrence and time to last event come from the El Paso Peaks area, just northwest of our station Johannesburg (JOBU, Figure 6). Two events are documented there during the last 550 years, and one may be as young as 200 years; recurrence interval estimates range from 700 to 1200 years and, in either case, are not highly periodic [*McGill and Rockwell*, 1998]. These uncertainties prevent exact knowledge of how the current state of the Garlock fault fits into simple viscoelastic fault slip models which rely on periodic recurrence intervals and a constraint on time since last event [e.g., *Savage and Lisowski*, 1998]. It is tempting to argue that the Garlock fault is late in the interseismic cycle (e.g., 550 years into a 700 year recurrence time), and thus a simple elastic half space model will tend to underestimate the long-term slip rate [*Thatcher*, 1983; *Savage and Lisowski*, 1998; *Dixon et al.*, 2000]. This relatively simple approach is flawed, however. The shorter recurrence estimate (700 years) comes from including all possible events, in particular the ambiguous 200-300 year event. If the most recent earthquake was 550 years ago, then the recurrence interval is longer than 700 years, and as much as 1200 years.

Also, block rotations as well as fault rotation could play a role in explaining the misfit of the Garlock fault slip rate. On geologic grounds the eastern Garlock fault is known to rotate, together with the blocks that bound it [*Burbank and Whistler*, 1987; *Jones*, 1987; *Dokka and Travis*, 1990a; *McGill and Sieh*, 1993; *Schermer et al.*, 1996]. This is consistent with our results that show concentration of deformation across the Blackwater-Calico fault that transects the Garlock fault without regional-scale offset (Plate 1 and Figure 5). Both structures are active at similar orders of magnitude and result in ongoing, mutual deformation. The deformation of the Garlock fault at its eastern end is a key element of Garlock fault kinematics and is consistent with geologic relations.

A transition in Eastern California shear zone kinematics lies to the south of the Northeast Mojave domain, where deformation is distributed across east-west striking sinistral faults before it passes across the Garlock fault. The Garlock fault itself is not a kinematic barrier between the Mojave Desert block and Walker Lane portions of the Eastern California shear zone. Rather, it is deformed by 4 mm/yr of dextral shear along the Blackwater, Goldstone Lake, and similar faults across the central Garlock fault and by rotation of the northeastern Mojave block. Dextral slip from the central Mojave Desert block is passed to the Owens Valley fault zone, primarily along faults in the Indian Wells Valley [*Roquemore and Simila*, 1994], Searles Valley and Death Valley regions (Figure 7).

4.3. Pattern and Magnitude of Deformation North of the Garlock Fault

North of the Garlock fault, eastern California dextral shear is concentrated within several large structural basins that contain the Owens Valley, Panamint-Hunter Mountain, and Death Valley-Fish Lake Valley faults (Figure 7). The oblique orientation of these features relative to plate margin shear results in pronounced extension and basin formation. For example, the Owens Valley fault composes part of the Sierra Nevada range front, a paired system of dextral and normal faults; the nearby Independence fault accommodates most of the range front normal fault motion [*Beanland and Clark*, 1994]. Such faults partition dextral and normal slip at the surface and merge at depth, commonly at the valley fill–bedrock interface, forming a single oblique-slip fault [*Armijo et al.*, 1989].

Although all three systems, the Owens Valley, Panamint-Hunter Mountain, and Death Valley-Fish Lake Valley fault zones, are active based on offset Quaternary features and seismicity, there is some uncertainty on their respective roles in accommodating Eastern California shear zone deformation. This partly reflects the uncertainty of estimating fault slip rates from geodetic data when the faults are closely spaced and their strain fields overlap and partly reflects the influence of the earthquake cycle [*Savage and Lisowski*, 1998]. On the basis of geologic evidence for active faulting within and near Death Valley, *Dokka and Travis* [1990] argued for significant partitioning of slip on the Death Valley-Furnace Creek fault zones. *Reheis and Sawyer* [1997] similarly argue for a significant late Quaternary slip rate for the Fish Lake Valley fault zone. Local geologic determinations yield only 2±1 mm/yr slip rate for the Owens Valley fault [*Beanland and Clark*, 1994].

Thus geological studies suggest a relatively fast eastern component (Death Valley-Furnace Creek-Fish Lake Valley fault zones) and a relatively slow western component (Owens Valley fault zone). In contrast, geodetic results favor higher slip rates in the west [*Gan et al.*, 2000; *this study*] and lower slip rates in the east [*Bennett et al.*, 1997; *Gan et al.*, 2000; *this study*].

4.3.1. Owens Valley fault. Holocene vertical offsets on the Lone Pine rupture and a characteristic ratio of vertical to horizontal slip during the 1872 earthquake point to a maximum slip rate of 2±1 mm/yr [*Beanland and Clark*, 1994]. Although the ages used in the rate calculation are not well determined, surface ages on varnished fans would have to be improbably young to support a higher slip rate. In addition, only three Holocene events are recognized, including the 1872 earthquake [*Beanland and Clark*, 1994], although these are on subsidiary traces of the Owens Valley fault. These relations have been taken to imply a recurrence interval of approximately 3500-5000 [*Beanland and Clark*, 1994].

Near-field trilateration data indicate strain accumulation equivalent to ~3 mm/yr of differential motion across Owens Valley [*Savage and Lisowski*, 1995]. When convolved with an elastic half space model, these rates of deformation suggest 6-7 mm/yr of long-term fault slip rate, in significant disagreement with the geological results. GPS results across longer baselines corroborate the EDM, with rates that increase with baseline length (Table 3; see also *Gan et al.* [2000]). A relative velocity of 7.6 mm/yr occurs between the west flank of the Sierra Nevada and the Darwin plateau (CEDA-5445, Figure 7). While as much as 1 mm/yr of this relative motion may be ascribed to the eastward decrease in San Andreas entrainment, when combined with an elastic model for the Owens Valley fault, a rate of 7 mm/yr is implied. If this reflects the long term rate, the recharge time for an 1872 type event with a coseismic dextral offset of 4-6 meters is 570 to 860 years; such displacement would require a dozen or more large Holocene events, only three of which are documented at Lone Pine Creek.

The Owens Valley fault last ruptured in 1872. Given that this fault may have recurrence times longer than 1000 years, it

is in the early stages of its earthquake cycle, in contrast with the eastern faults, which are probably in the late stages. Postseismic effects associated with the viscoelastic response of the lower crust/upper mantle may explain at least part of the discrepancy [*Dixon et al.*, 2000].

4.3.2. Panamint-Hunter Mountain faults. *Burchfiel et al.* [1987] suggest a geologic model for the opening of Panamint Valley along a stepped normal (Panamint Valley) and strike-slip (Hunter Mountain) fault at 2-3 mm/yr over the last 4 Myr, based on geologic mapping of the northern end of Panamint Valley. Saline Valley, to the north of the Hunter Mountain fault, is a part of this system. Similarly, prehistoric surface ruptures in southern Panamint Valley show partitioning of normal offset against the range front and an oblique (dextral and normal) fault system offsetting alluvial and pluvial features west of the range front [*Zhang et al.*, 1990]. The oblique system consists of both normal and dextral ruptures that indicate a more northerly integrated slip vector (N35°W) than that implied by the orientation of the Hunter Mountain fault (N60°W) [*Zhang et al.*, 1990]. Slip rates from both studies agree at the ~2 mm/yr level and are consistent with the data we present here. The azimuth of the GPS velocities for baselines that cross the fault are parallel to the Hunter Mountain fault and confirm the geologic model that calls for strike slip along this structure and oblique opening of Panamint Valley [*Burchfiel et al.*, 1987]. These results are also consistent with other recent high-precision GPS studies [*Bennett et al.*, 1997; *Gan et al.*, 2000].

4.3.3. Death Valley-Furnace Creek fault zone and the Fish Springs Valley fault. A total of 30 km offset has occurred during the last 3-5 Myr along the Death Valley fault zone [*Hamilton and Myers*, 1966]. This suggests a slip rate of 3 mm/yr, which broadly agrees with rates determined from an alluvial fan, inferred to be post-mid Miocene and pre-1 Ma, that is offset 35 km by the southern Death Valley fault zone [*Butler et al.*, 1988]. No absolute dates yet exist to precisely constrain the slip rate. To the north the Death Valley fault zone passes along strike into the Fish Lake Valley fault, which is well studied and is inferred to slip 4 mm/yr since the late Pleistocene [*Reheis and Sawyer*, 1997], and is consistent with recent GPS determinations of 3-5 mm/yr [*Bennett et al.*, 1997; *Gan et al.*, 2000]. Our study agrees with 5 mm/yr along the Death Valley fault zone.

GPS-determined kinematics demonstrate a budget of ~13 mm/yr for the Eastern California shear zone north of the Garlock fault, greater than suggested by geologic constraints, yet consistent with independent estimates of fault slip rates from other geodetic studies and techniques. This increased slip rate budget on the Owens Valley fault in particular and for the Eastern California shear zone as a whole exceeds paleoseismic estimates but is consistent with independent geodetic studies from smaller regions [*Savage and Lisowski*, 1995; *Bennett et al.*, 1997; *Gan et al.*, 2000].

5. Conclusions

The GPS results presented here reveal the modern deformation field within the Eastern California shear zone. Whereas the direction of motion is similar to that predicted from previous geologic estimates, the magnitude of measured slip rates is greater. The kinematic consequences of this deformation refine constraints on the role of continental margin deformation in accommodating relative plate motion.

1. The total fault slip budget within the Eastern California shear zone, while variable along strike, is greater everywhere than previously appreciated and accounts for 28-29% of the relative motion between the North America and Pacific plates.

2. Our GPS network experiences coherent motion relative to stable North America. Some of this motion can be ascribed to entrainment in the elastic deformation field of the San Andreas fault, which maps into Nevada if current elastic deformation models are employed. Some of the coherent motion of the network, of the order of a millimeter per year, is ascribed to deformation farther to the east, including the Basin and Range. These deformation sources contribute to reconciling earlier discrepancies in fault slip distribution budgets.

3. On a plate margin scale the shear zone is characterized by distributed deformation across a belt that varies from tens to hundreds of kilometers in width. Within certain structural domains, the GPS results limit the slip rates of individual faults within the deforming zone.

4. Within the Mojave Desert block the total budget of plate motion parallel dextral slip is 14 mm/yr. In the southern Mojave Desert, this slip is confined to a narrow zone that merges with the San Andreas fault north of the Salton Sea. In the central Mojave Desert, modern slip is concentrated along a few medial faults. During the 1993-1998 observation interval, some motion at particular stations in this region is likely related to transient deformation in the wake of the 1992 Mw = 7.3 Landers earthquake. North of Barstow, California, some slip steps eastward through the Northeast Mojave domain, although less than has been inferred from previous VLBI-based estimates. About half of the 14 mm/yr passes over the central Garlock along the Blackwater and perhaps the Goldstone Lake faults.

5. Along-strike and across-strike differences in the distribution of Eastern California shear zone-related deformation imply that the Garlock fault separates structural domains with differing loci of plate margin extension. How dextral, northwest directed slip passes across the Garlock fault itself implies a mechanism for deformation of its eastern end. To first order these results are consistent with geological models that propose clockwise rotation of the eastern Garlock fault from its original more northeasterly orientation. The data are also consistent with the notion that the Garlock fault is deformed by the Panamint or nearby fault zones and the Blackwater or Goldstone Lake fault zone.

6. North of the Garlock fault, the integrated slip rate budget is smaller (13 mm/yr) and is partitioned on several faults such that about half of the modern slip (7 mm/yr) occurs on faults within Owens Valley; the other 6 mm/yr are divided among faults within Panamint Valley and Death Valley. The azimuth of the cumulative relative motion lies counterclockwise from the strike of local faults, creating Basin and Range topography. It also lies slightly clockwise from the relative plate motion direction, implying ongoing extension of the plate margin. The estimate of 13 mm/yr on faults within this part of the Eastern California shear zone agrees with recent estimates of Sierra Nevada block motion from an overlapping data set [*Dixon et al.*, 2000] because ~1 mm/yr of its 14 mm/yr lies farther east than the faults considered here.

7. Disagreement between geodetic and geologic results persist for the Owens Valley fault and the Garlock fault. Geodetic results convolved with a simple elastic model overestimate geologic slip rates on the Owens Valley fault by a factor of 3. In the case of the Garlock fault, the geodesy and simple

elastic model underestimate geologic slip rates by a factor of 3. In both cases, the geologic and geodetic data sets are of high quality, although better geologic slip rate determinations over a range of time scales are needed in Owens Valley. Reconciliation of these discrepancies implies either real differences in rates over decade vs. geologic time scales, or inadequacies in the slip models, or both.

Previous attempts to construct a budget for plate margin deformation from geologic data need to be reevaluated in light of these refined constraints. The kinematic consequences of these results imply a larger geodetic moment budget for the Eastern California shear zone than previously determined. If all the accumulating strain is released coseismically, recurrence intervals for a Landers or Owens Valley type earthquake on the Eastern California shear zone as a whole are respectively 285 and 500 years for any particular transect with a width equivalent to the 70-100 km long, along-strike rupture length.

Acknowledgments. The National Aeronautics and Space Administration supported this work through Dynamics of the Solid Earth Program grants to M. M. Miller and T. H. Dixon. The National Science Foundation supplied GPS equipment through an ILI grant to M. M. Miller. The project relied on the generous efforts of numerous field volunteers over the years: August 1993, Carol Dupuis, Dan Casper, Tracy Grover, Rick Heath, Jim Hooper, Ann Jensvold, Joshua Lovett, Lori Rome, David Townsend, Chris Walls, and Suzanne Yarbrough; September 1994, Simona Errico, Susanna Gross, Leslie Jackson, Joe Martinez, Carolyn McCarthy, Hongzhi Wang, and Carrie Whitehill; September-October 1995, Karl Feaux, Terry Frost, Tim Gere, Tracy Grover, Karen Hansen, Lina Hellman, Rowena Lohman, Kim McClean, Giovanni Sella, Sarah Ann Touliatos, Mark Treick, Hongzhi Wang, and Carrie Whitehill; September 1996, Doug Anderson, Ken Austin, Will Blanton, Tim Gere, Dan Johnson, Cindy Kissler, Lisa Steubing, and Chaz Wichman; June-July 1997, Doug Anderson, Kyle Antonelis, Ken Austin, Shane Martin, Forrest Roberts, Sam VanLaningham, and Todd Williams; June-July 1998, Taylor Everett, Erik Johansen, Addie Sullivan, Sam VanLaningham, Janet Vaughn, and Todd Williams; December 1998, Sam VanLaningham and Todd Williams. In addition, field support was provided by UNAVCO personnel and CWU field experiment managers: Ken Austin, Karl Feaux, Bjorn Johns, Dan Johnson, Ed Manzanares, Sam VanLaningham, Todd Williams, and Carrie Whitehill. Special thanks to Steve Fisher who installed stations and supported this project in many roles over the years at JPL and UNAVCO. Additional data were incorporated from several sources including continuous stations that are operated by the Bay Area Regional Deformation Array (BARD), the Geothermal Program Office of the U.S. Navy, NASA, and the Southern California Integrated GPS Network (SCIGN). Discussions with Brad Hager, Tom Herring, Robert King, Gene Humphreys, Elizabeth Hearn, Simon McClusky, and Brendon Meade improved the manuscript. Chuck DeMets kindly provided code to define North America in a GPS reference frame. Simon McClusky provided generous assistance with GAMIT/GLOBK postprocessing tools. Todd Williams compiled the DEM and assisted in developing the GMT [*Wessel and Smith*, 1995] figures. Comments on the manuscript by Jim Savage and an anonymous reviewer are gratefully acknowledged.

References

Argus, D.F., and R.G. Gordon, Tests of the rigid-plate hypothesis and bounds on intraplate deformation using geodetic data from Very Long Baseline Interferometry, *J. Geophys. Res.*, *101*, 13,555-13,572, 1996.

Armijo, R., P. Tapponnier, and T. H, Late Cenozoic right-lateral strike-slip faulting in southern Tibet, *J. Geophys. Res.*, *94*, 2787–2838, 1989.

Astiz, L., and C.R. Allen, Seismicity of the Garlock fault, California, *Bull. Seismol. Soc. Am.*, *73*, 1721-1734, 1983.

Atwater, T., Implications of plate tectonics for the Cenozoic tectonic evolution of western North America, *Bull. Geol. Soc. Am.*, *81*, 3513-3536, 1970.

Atwater, T., and J. Stock, Pacific-North America plate tectonics of the Neogene southwestern United States: An update, *International Geology Review*, *40*, 375-402, 1998.

Beanland, S., and M.M. Clark, The Owens Valley fault zone, eastern California, and surface faulting associated with the 1872 Earthquake, *U.S. Geol. Surv. Bull.*, *1982*, 29 pp., 1994.

Bennett, R.A., W. Rodi, and R.E. Reilinger, Global Positioning System constraints on fault slip rates in southern California and northern Baja California, Mexico, *J. Geophys. Res.*, *101*, 21,943-21,960, 1996.

Bennett, R.A., B.P. Wernicke, J.L. Davis, P. Elosegui, J.K. Snow, M.J. Abolins, M.A. House, G.L. Stirewalt, and D.A. Ferrill, Global Positioning System constraints on fault slip rates in the Death Valley region, California and Nevada, *Geophys. Res. Lett.*, *24*, 3073-3076, 1997.

Bird, P., and R.W. Rosenstock, Kinematics of present crust and mantle flow in southern California, *Bull. Geol. Soc. Am.*, *95*, 946-957, 1984.

Bock, Y., S. et al., Southern California Permanent GPS Geodetic Array: Continuous measurements of regional crustal deformation between the 1992 Landers earthquake and 1994 Northridge earthquake, *J. Geophys. Res.*, *102*, 18,013-18,033, 1997.

Boucher, C., Z. Altamimi, M. Reissel, and P. Sillard, Results and analysis of the ITRF96, Central Bureau of IERS, Obs. de Paris, Paris, 1998.

Burbank, D.W., and D.P. Whistler, Temporally constrained tectonic rotations derived from magnetostratigraphic data: Implications for the initiation of the Garlock Fault, California, *Geology*, *15*, 1172-1175, 1987.

Burchfiel, B.C., K.V. Hodges, and L.H. Royden, Geology of Panamint Valley-Saline Valley pull-apart system, California: Palinspastic evidence for low-angle geometry of a Neogene range-bounding fault, *J. Geophys. Res.*, *92*, 10,422-10,426, 1987.

Butler, P.R., B.W. Troxel, and K.L. Verosub, Late Cenozoic history and styles of deformation along the southern Death Valley fault zone, California, *Bull. Geol. Soc. Am.*, *100*, 402-410, 1988.

Davis, G.A., and B.C. Burchfiel, Garlock fault: An intracontinental transform structure, southern California, *Bull. Geol. Soc. Am.*, *84*, 1407-1422, 1973.

DeMets, C., R. G. Gordon, S. Stein, and D. F. Argus, A revised estimate of Pacific-North America motion and implications for western North America plate boundary zone tectonics, *Geophys. Res. Lett.*, *14*, 911-914, 1987.

DeMets, C., A reappraisal of seafloor spreading lineations in the Gulf of California: Implications for the transfer of Baja California to the Pacific plate and estimates of Pacific-North America motion, *Geophys. Res. Lett.*, *22*, 3545-3548, 1995.

DeMets, C., and T.H. Dixon, Kinematic models for Pacific-North America motion from 3 Ma to present, I: Evidence for steady motion and biases in the NUVEL-1A model, *Geophys. Res. Lett.*, *26*, 1921-1924, 1999.

DeMets, C., R.G. Gordon, D.F. Argus, and S. Stein, Current plate motions, *Geophys. J. Int.*, *101*, 425-478, 1990.

DeMets, C., R.G. Gordon, D.F. Argus, and S. Stein, Effect of recent revisions to the geomagnetic reversal time-scale on estimates of current plate motions, *Geophys. Res. Lett.*, *21*, 2191-2194, 1994.

Dixon, T.H., S. Robaudo, J. Lee, and M.C. Reheis, Constraints on present-day Basin and Range deformation from space geodesy, *Tectonics*, *14*, 755-772, 1995.

Dixon, T.H., M.M. Miller, F. Farina, H. Wang, and D.J. Johnson, Present-day motion of the Sierra Nevada block, and some implications for Basin and Range tectonics, *Tectonics*, *19*, 1-24, 2000.

Dokka, R.K., Displacements on Late Cenozoic strike-slip faults of the central Mojave Desert, California, *Geology*, *11*, 305-308, 1983.

Dokka, R.K., Patterns and modes of early Miocene extension of the central Mojave Desert, California, in *Continental Extension Processes*, edited by L. Mayer, pp. 75-95, Geol. Soc. of Am., Boulder, Colo., 1986.

Dokka, R.K., The Mojave extensional belt of southern California, *Tectonics*, *8*, 363-390, 1989.

Dokka, R.K., The Eastern California shear zone and its role in the creation of young extensional zones in the Mojave Desert, in *Structure, Tectonics and Mineralization of the Walker Lane*, edited by S.D. Craig, pp. 161-187, Geol. Soc. of Nev., Reno, 1993.

Dokka, R.K., and C.J. Travis, Late Cenozoic strike-slip faulting in the Mojave Desert, California, *Tectonics*, *9*, 311-340, 1990a.

Dokka, R.K., and D.J. Travis, Role of the Eastern California shear zone in accommodating Pacific-North American plate motion, *Geophys. Res. Lett.*, *17*, 1323-1326, 1990b.

Dokka, R.K., T.M. Ross, and G. Lu, The Trans Mojave-Sierran shear zone and its role in the Early Miocene collapse of southwestern North America, in *Continental Transpressional and Transtensional Tectonics*,

edited by R.E. Holdsworth, R.A. Strachan, and J.F. Dewey, pp. 183-202, Geol. Soc., London, 1998.

Du, Y., and A. Aydin, Is the San Andreas Big Bend responsible for the Landers earthquake and the eastern California shear zone?, *Geology*, *24*, 219-222, 1996.

Feigl, K.L., D.C. Agnew, Y. Bock, D. Dong, A. Donnellan, B.H. Hager, T.A. Herring, D.D. Jackson, and T.H. Jordan, Space geodetic measurement of crustal deformation in central and southern California, *J. Geophys. Res.*, *98*, 21,677-21,712, 1993.

Gan, W., J.L. Svarc, J.C. Savage, and W.H. Prescott, Strain accumulation across the Eastern California shear zone at latitude 36°30' N, *J. Geophys. Res.*, *105*, 16,229-16,236, 2000.

Garfunkel, Z., Model for the Late Cenozoic tectonic history of the Mojave Desert, California, and for its relation to adjacent regions, *Bull. Geol. Soc. Am.*, *85*, 1931-1944, 1974.

Gomberg, J., and M. Ellis, Topography and tectonics of the central New Madrid seismic zone: Results of numerical experiments using a three-dimensional boundary element program, *J. Geophys. Res.*, *99*, 20,299-20,310, 1994.

Hamilton, W.B., and W.B. Myers, Cenozoic tectonics of the western United States, *Rev. Geophys*, *4*, 509-549, 1966.

Hearn, E.H., and E.D. Humphreys, Kinematics of the southern Walker Lane belt and motion of the Sierra Nevada block, California, *J. Geophys. Res.*, *103*, 27,033-27,049, 1998.

Humphreys, E.D., and R.J. Weldon, Deformation across the western United States: A local estimate of Pacific-North America transform deformation, *J. Geophys. Res.*, *99*, 19,975-20,010, 1994.

Jennings, C.W., Fault activity map of California and adjacent areas with locations and ages of recent volcanic eruptions, Calif. Div. of Mines and Geol., Dep. of Conserv., Sacramento, 1994.

Johnson, H.O., and D.C. Agnew, Monument motion and measurement of crustal velocities, *Geophys. Res. Lett.*, 22, 2905-2908, 1995.

Jones, C.H., Is extension in Death Valley accommodated by thinning of the mantle lithosphere beneath the Sierra Nevada, California?, *Tectonics*, *6*, 449-473, 1987.

Kanamori, H., H.K. Thio, D. Dreger, E. Hauksson, and T. Heaton, Initial investigation of the Landers, California, Earthquake of 28 June 1992 using TERRAscope, *Geophys. Res. Lett.*, *19*, 2267-2270, 1992.

Kenner, S.J., and P. Segall, Post-seismic deformation following the 1906 San Francisco earthquake, *J. Geophys. Res.*, *105*, 13,195-13210, 2000.

King, N.E., Horizontal deformation in the Mojave Desert near Barstow, California, 1979-1983, *J. Geophys. Res.*, *90*, 4491-4494, 1985.

Langbein, J., and H. Johnson, Correlated errors in geodetic time series: Implications for time dependent deformation, *J. Geophys. Res.*, *102*, 591-603, 1997.

Larson, K.M., J.T. Freymueller, and S. Philipsen, Global plate velocities from the Global Positioning System, *J. Geophys. Res.*, *102*, 9961-9981, 1997.

Loomis, D.P., and D.W. Burbank, The stratigraphic evolution of the El Paso basin, southern California: Implications for the Miocene development of the Garlock fault and uplift of the Sierra Nevada, *Bull. Geol. Soc. Am.*, *100*, 12-28, 1988.

Luyendyk, B.P., M.J. Kamerling, and R. Terres, Geometric model for Neogene crustal rotations in southern California, *Bull. Geol. Soc. Am.*, *91*, 211-217, 1980.

MacConnell, D.F., C. McCabe, R.K. Dokka, and M. Chu, Paleomagnetic and structural evidence for localized tectonic rotation associated with fault drag in the northeastern Mojave Desert: Implications for the late Cenozoic tectonic evolution of the Eastern California shear zone, *Earth Plan. Sci. Lett.*, *126*, 207-216, 1994.

Mao, A., C.G.A. Harrison, and T. Dixon, Noise in GPS coordinate time series, *J. Geophys. Res.*, *104*, 2797-2816, 1999.

McGill, S., and T. Rockwell, Ages of late Holocene earthquakes on the central Garlock fault near El Paso Peaks, California, *J. Geophys. Res.*, *103*, 7265-7279, 1998.

McGill, S.F., and K. Sieh, Surficial offsets on the central and eastern Garlock fault associated with prehistoric earthquakes, *J. Geophys. Res.*, *96*, 21,597-21,621, 1991.

McGill, S.F., and K.E. Sieh, Holocene slip-rate of the central Garlock fault in southeastern Searles Valley, California, *J. Geophys. Res.*, *98*, 14,217-14,231, 1993.

Miller, M.M., M.P. Golombek, R.K. Dokka, and S. Fisher, Distribution of contemporary slip in the Mojave Desert and Walker Lane: A Global Positioning System (GPS) experiment, in *Deformation Associated with the Neogene Eastern California Shear Zone, Southeastern California and Southwestern Arizona*, edited by S.M. Richard, pp. 59-63, San Bernardino County Mus., Redlands, Calif., 1992.

Miller, M.M., F. Webb, D. Townsend, M.P. Golombek, and R.K. Dokka, Regional coseismic deformation from the June 28, 1992, Landers, California, earthquake: Results from the Mojave GPS network, *Geology*, *21*, 868-872, 1993.

Monastero, F.C., A.E. Sabin, and J.D. Walker, Evidence for post-early Miocene initiation of movement on the Garlock fault from offset of the Cudahy Camp Formation, east-central California, *Geology*, *25*, 247-250, 1997.

Petersen, M.D., and S.G. Wesnousky, Review: Fault slip rates and earthquake histories for active faults in southern California, *Bull. Seismol. Soc. Am.*, *84*, 1,608-1,649, 1994.

Pezzopane, S.K., and R. Weldon, Tectonic role of active faulting in central Oregon, *Tectonics*, *12*, 1140-1169, 1993.

Reheis, M.C., and T.L. Sawyer, Late Cenozoic history and slip rates of the Fish Lake Valley, Emigrant Peak, and Deep Springs fault zones, Nevada and California, *Bull. Geol. Soc. Am.*, *109*, 280-299, 1997.

Rockwell, T.K., D.P. Schwartz, K. Sieh, C. Rubin, S. Lindvall, M. Herzberg, D. Padgett, and T. Fumal, Initial paleoseismic studies following the Landers earthquake: Implications for fault segmentation and earthquake clustering., *Eos Trans. AGU*, *74*, *Fall Meet. Suppl.*, 67, 1993.

Roquemore, G.R., and G.W. Simila, Aftershocks from the 28 June 1992 Landers earthquake: Northern Mojave Desert to the Coso Volcanic Field, California, *Bull. Seismol. Soc. Am.*, *84*, 854-862, 1994.

Rubin, C.M., and K. Sieh, Long dormancy, low slip rate and similar slip-per-event for the Emerson fault, Eastern California shear zone, *J. Geophys. Res.*, *102*, 15,319-15,333, 1997.

Sauber, J., M. Lisowski, and S.C. Solomon, Geodetic measurement of deformation east of the San Andreas fault in central California, in *Slow Deformation and Transmission of Stress in the Earth, Geophys. Monogr. Ser.*, vol. 49, edited by S.C. Cohen and P. Vanicek, AGU, Washington, D.C., 71-86, 1989.

Sauber, J., W. Thatcher, S.C. Solomon, and M. Lisowski, Geodetic slip rate for the eastern California shear zone and the recurrence time of Mojave desert earthquakes, *Nature*, *367*, 264-266, 1994.

Savage, J.C., M. Lisowski, and W.H. Prescott, An apparent shear zone trending north-northwest across the Mojave Desert into Owens Valley, eastern California, *Geophys. Res. Lett.*, *17*, 2113-2116, 1990.

Savage, J.C., and M. Lisowski, Strain accumulation in Owens Valley, California, 1974-1988, *Bull. Seismol. Soc. Am.*, *85*, 151-158, 1995.

Savage, J.C., and M. Lisowski, Viscoelastic coupling model of the San Andreas fault along the Big Bend, southern California, *J. Geophys. Res.*, *103*, 7281-7292, 1998.

Schermer, E.R., B.P. Luyendyk, and S. Cisowski, Late Cenozoic structure and tectonics of the northern Mojave Desert, *Tectonics*, *15*, 905-932, 1996.

Scientists from the U.S. Geological Survey, S.C.E.C., and California Division of Mines and Geology, Preliminary report on the 16 October 1999 M 7.1 Hector Mine, California, earthquake, *Seismol. Res. Lett.*, *71*, 11-23, 2000.

Shen, Z.-K., L.-Y. Sung, D. Dong, B. King, T. Herring, S. McClusky, and K. Hudnut, Southern California Earthquake Center, Horizontal deformation velocity map Version 2.0, http://quakedc.gps.caltech.edu :3128/group_e/release.v2/index.html, Southern California Earthquake Center, Pasadena, California, 1998.

Sieh, K.E., and R. Jahns, Holocene activity of the San Andreas fault at Wallace Creek, California, *Bull. Geol. Soc. Am.*, *95*, 883-896, 1984.

Sieh, K., M. Stuiver, and D. Brillinger, A more precise chronology of earthquakes produced by the San Andreas fault in southern California, *J. Geophys. Res.*, *94*, 603-623, 1989.

Sillard, P., Z. Altamimi, and C. Boucher, The ITRF96 realization and its associated velocity field, *Geophys. Res. Lett.*, *25*, 3223-3226, 1998.

Spotila, J.A., and K. Sieh, Architecture of transpressional thrust faulting in the San Bernardino Mountains, southern California, from defomation of a deeply weathered surface, *Tectonics*, *19*, 589-615, 2000.

Stock, J.M., and P. Molnar, Uncertainties and implications of the Late Cretaceous and Tertiary position of North America relative to the Farallon, Kula, and Pacific plates, *Tectonics*, *7*, 1339-1384, 1989.

Thatcher, W., Nonlinear strain buildup and the earthquake cycle on the San Andreas Fault, *J. Geophys. Res.*, *88*, 5893-5902, 1983.

Thatcher, W., G.R. Fougler, B.R. Julian, J. Svarc, E. Quilty, and G.W. Bawden, Present day deformation across the Basin and Range province, *Science*, *283*, 1714-1718, 1999.

Unruh, J.R., R.J. Twiss, and E. Hauksson, Seismogenic deformation field

in the Mojave block and implications for tectonics of the eastern California shear zone, *J. Geophys. Res.*, *101*, 8335-8361, 1996.

Wallace, R.E., Patterns and timing of late Quaternary faulting in the Great Basin Province and relation to some regional tectonic features, *J. Geophys. Res.*, *89*, 5763-5769, 1984.

Ward, S.N., Pacific-North America plate motions: New results from very long baseline interferometry, *J. Geophys. Res.*, *95*, 21,965-21,981, 1990.

Wdowinski, S., Y. Bock, J. Zhang, P. Fang, and J. Genrich, Southern California Permanent GPS Geodetic Array: Spatial filtering of daily positions for estimating coseismic and postseismic displacements induced by the Landers earthquake, *J Geophys. Res*, *102*, 18,057-18,070, 1997.

Weldon, R., and E. Humphreys, A kinematic model of southern California, *Tectonics*, *5*, 33-48, 1986.

Weldon, R.J., and K.E. Sieh, Holocene rate of slip and tentative recurrence interval for large earthquakes on the San Andreas fault in Cajon Pass, southern California., *Bull. Geol. Soc. Am.*, *96*, 793-812, 1985.

Wessel, P., and W.H.F. Smith, New version of the Generic Mapping Tools released, *Eos, Trans. AGU*, *76*, Fall Suppl., 329, 1995.

Zhang, J., Y. Bock, H. Johnson, P. Fang, S. Williams, S. Wdowinski, J. Behr, and J.F. Genrich, Southern California permanent GPS geodetic array: Error analysis of daily position estimates and site velocities, *J. Geophys. Res.*, *102*, 18,035-18,055, 1997.

Zhang, P., M. Ellis, D.B. Slemmons, and F. Mao, Right-lateral displacements and the Holocene slip rate associated with prehistoric earthquakes along the southern Panamint Valley fault zone: Implications for southern Basin and Range tectonics and coastal California deformation, *J. Geophys. Res.*, *95*, 4857-4872, 1990.

Zumberge, J., M.B. Heflin, D.C. Jefferson, M.M. Watkins, and F.H. Webb, Precise point positioning for the efficient and robust analysis of GPS data from large networks, *J. Geophys. Res.*, *102*, 5005-5017, 1997.

T. H. Dixon, Division of Marine Geology and Geophysics, Rosentiel School of Marine and Atmospheric Sciences, University of Miami, 4600 Rickenbacker Causeway, Miami, FL 33149. (tdixon@rsmas.miami.edu)

R. K. Dokka, Department of Geology and Geophysics, Louisiana State University, Baton Rouge, LA 70803. (rkdokka@biotite.geol.lsu.edu)

D. J. Johnson and M. M. Miller, Department of Geological Sciences, Central Washington University, 400 E. Eighth Avenue, Ellensburg, WA 98926. (meghan@geology.cwu.edu; dan@geology.cwu.edu)

(Received May 14, 1999; revised July 15, 2000;
accepted August 23, 2000.)